12-2016

Relationship Between Velocity of Contraction and Force Applied On Air Muscles

Aniruddha Sudhir Phatak
asp2209@rit.edu

Relationship Between Velocity of Contraction and Force Applied On Air Muscles

by

Aniruddha Sudhir Phatak

A Thesis Submitted in Partial Fulfillment of the Requirements for the degree of Master of Science in Mechanical Engineering.

Supervised by
Dr. Steven Day, Associate Professor
Department of Mechanical Engineering
Kate Gleason College of Engineering
Rochester Institute of Technology
Rochester, New York

December, 2016

Approved by:

_____

Dr. Steven Day, Associate Professor
Thesis Advisor, Department of BioMedical Engineering

_____

Dr. Kathleen Lamkin-Kennard, Associate Professor
Committee Member, Department of Mechanical Engineering

_____

Dr. Wayne Walter, Professor
Committee Member, Department of Mechanical Engineering

_____

Dr. Agamemnon Crassidis, Professor
Department Representative, Department of Mechanical Engineering

Thesis Release Permission Form

Rochester Institute of Technology
Kate Gleason College of Engineering

Title:

Relationship Between Velocity of Contraction and Force Applied on Air Muscles

I, Aniruddha Phatak, hereby grant permission to the Wallace Memorial Library to reproduce my thesis in whole or part.

_____

Aniruddha Sudhir Phatak

_____

Date:

.

Acknowledgements

I would like to extend my sincere thanks to my advisor, Dr. Steven Day for his guidance, knowledge and continual support throughout my theoretical and experimental research which helped me to complete my thesis.

I would also like to thank my friend Shahan who helped me with the LabVIEW Programming.

I would like to thank Drs. Wayne Walter and Kathleen Lamkin-Kennard for providing advice and material support, including air muscle supplies and instrumentation. I am also thankful to Mr. Jan Maneti, Mr. Rob Kraynik, and Carmen Azzaretti for helping me in the manufacturing of my test rig.

Lastly, I would like to thank my parents, Mr. Sudhir Phatak and Mrs. Chitra Phatak for their tremendous support and strong motivation throughout my life.

.

Abstract

Air muscles are simple pneumatic devices that have high potential to be used as robotic manipulators, as they have a behavior similar to biological motors or muscles. Hence, they have a wide range of potential applications in areas such as robotics, bio-robotics, biomechanics, and artificial limb replacements. In addition to the similarity to biological muscle, air muscles have the advantages of good power-to-weight ratio, being compliant, and low cost. This thesis primarily quantifies the relationship between velocity of contraction of air muscles and the force applied on it, which is a key characteristic of biological skeletal muscle. First, an experimental test rig was used to measure the velocity of contraction of air muscles as a function of applied force, supply pressure, and supply volumetric flow rate. Second, a theoretical model is proposed to quantify the relationship between the velocity of contraction and force applied on it and to explain the experimental results.

Three air muscles having different lengths and diameters were tested for loads ranging from 0 to 6 kg at 20 psi, 40 psi and 60 psi at two different flow rates. All three air muscles were made up of latex tubing sheathed with the *Techflex*, *FlexoPet* braided sleeve. The primary air muscle was 5 inches long, with the diameter of the inner tube measuring 3/4 of an inch. The second muscle had half the length (2.5 inches) and was the same diameter as the primary air muscle. The third air muscle was the same length as the first (5 inches long), but half of the diameter (3/8 of an inch). The velocity of the contraction was measured with the help of the linear potentiometer.

Both the theoretical model and the experimental results found that as the force applied on the air muscles is increased, maximum length of contraction and velocity of contraction decrease. Both model and experiment showed that the velocity of contraction increases as a function of both pressure and volume flow rate.

.

Contents:

.

.

Nomenclature:

PAM = Pneumatic Artificial Muscle

PPAM = Pleated Pneumatic Artificial Muscle

P = absolute gas pressure

P_0 = atmospheric pressure

F = force

P' = relative internal gauge pressure

s_i = total inner surface

ds_i = the area vector

dl_i = inner surface displacement

dV = volume change.

D = diameter of Air Muscle at particular position

D_0 = diameter of the air muscle at normal position

b = braided length of the air muscle

θ = braided angle at a specific position

L = contracted length of Air Muscle

L_0 = normal length of Air Muscle

L_s = stretched length of Air Muscle

tk= thickness of the air muscle (shell and bladder)

n = number of turns of the thread

C = Circumference

N_c = number of nodes

I = inter strand separation

.

G = distance between two nodes

D_s = diameter of one strand

W_B = width of each strand

N = number of strands

N_c = number of nodes in one circulation of the circumference

S = number of parallel strands

L_{min} = minimum length of muscle at maximum contraction

c = compliance

k = stiffness

R_{min} = minimum radius of air muscle

ε = strain

a = dimensionless factor for elasticity

$F_{friction}$ = resisting force caused due to Dry friction is air muscle

$S_{contact}$ = total contact area between the strands of whole muscle

$N_{conatcts}$ = total number of crossover points

S_{one} = area of one contact polygon

f_s = coefficient of friction

V = volume of air inside the air muscle

M = mass of air inside the air muscle

R = Restriction created by the needle valve *(Volume flow rate)*

$Mdot$ = Mass flow rate

.

List of Figures:

.

.

1. Introduction

An air muscle is a simple pneumatic device which was developed by J. L. Mckibben in the 1950s. It was primarily developed for polio patients as an orthotic appliance according to Baldwin [4, 7]. Initially, these muscles were made up of pure latex rubber. As they closely resemble the natural muscle when actuated by air, they became known as air muscles. In the late 1980s, the Bridgestone Rubber Company commercialized these rubber actuators, and since then, many types of air muscles have been used as manipulators mainly for prostheses and orthotics [4, 8]. A Mckibben Air muscle consists of a rubber bladder surrounded by a braided mesh shell which is attached to an air fitting on one end and two mechanical fittings at both ends. As the internal bladder is pressurized, it expands and pushes against the mesh to increase its volume. Due to high non-extensibility of the threads in the braided mesh shell, when activated, the air muscle's diameter increases and produces tension if coupled with a mechanical load, producing a contractive force.

One of the potential uses of air muscles include manufacturing of dexterous robotic hand having good control of all the fingers in order to fulfill basic hand operations like catching, picking, pulling, and placing objects. Another important application is to make an artificial leg that can walk, run, and jump like a human. Researchers Hannaford et al. built an Anthropomorphic Biorobotic Arm which consisted of fifteen Mckibben muscles [2, 9]. The main purpose was "to improve the understanding of the reflexive control of human movement and posture." Grodski and Immega [2, 10] used ROMACs to control a tele operated arm having one degree of freedom (dof) with the help of myoelectric signals generated from the human operator's triceps and biceps. Specific position and control over stiffness of the robot arm were achieved by regulating pressures of the ROAMCs proportional to EMG signal output. Bridgestone Co. [2, 8] developed a Soft Arm powered by Rubbertuators, which consisted of different parts like upper and lower arm, a shoulder, and a wrist that could perform operations like painting and coating. For all these applications, it is essential to study the force and velocity characteristics of air muscles.

.

1.1 Problem Statement:

Air Muscles are currently finding a place in a wide range of applications like robotics, bio-robotics, biomechanics, and artificial limb replacement. As the characteristics of air muscles resemble the skeletal muscles they can be used to perform high end hand applications like assembling of very minute components etc., once coupled with neural network systems and precise sensors. To achieve accurate positioning and gripping force in all these applications it is necessary to understand the relation between force exerted by the air muscle and its velocity of contraction.

I did not find any literature regarding velocity of contraction during my course of research. My research question primarily asks, what is the exact relationship between the force acting on the air muscle and the corresponding velocity of its contraction for varying air pressures and volume flow rates? Given this relationship, future designers can achieve specific force-velocity relationships, which will help development of biometic actuators. For example, we can achieve desired movement of the fingers or the legs to perform the required operations by knowing the mathematical equation force and velocity.

1.2 Objective:

1. To build a test rig which to measure the velocity of contraction of air muscles when different forces are applied by taking into account the effect of varying pressures and volume flow rates.
2. To propose a theoretical model to quantify the relationship between the velocity of contraction and the force applied and including the effect of varying pressures and volume flow rates in order to validate the experimental results.

.

2. Study of Air Muscles:

2.1. Nature of Air muscles

Pneumatic actuators are extensively used in automation industries. Lately pneumatics are widely used in robotics as the main source of power for achieving necessary motion. Compliant nature of pneumatics is of prime importance as robotics often deal with interaction between man and machine or between robots and delicate objects which are to be handled by robots. The compliant nature due to the compressibility of air and the control over operating pressure makes soft and safe interaction between pneumatically handled robots and the corresponding objects possible. Conventionally, hydraulic and electric drives were used in robotics. Unlike skeletal muscle, these systems often are fixed displacement systems that will move to a certain position regardless of the applied force. In order to obtain an actuator system with behavior that reacts to this load, these systems typically need complex feedback loop systems to attain the required compliant nature. Pneumatic Artificial Muscles (PAMs) can be considered as contractile and linear motion engines which are operated by air pressure. [2]

2.1.1. Compliant nature of Air muscles: [2]

Pneumatic actuators show compliant nature because of compressibility of the gas. Change in force is directly proportional to change in length when pressure is maintained constant, so the PAM behaves like a spring. Compliance, c is given as-

$$c^{-1} = K = \frac{dF}{dL} = -\frac{dp'}{dV}\left(\frac{dV}{dL}\right)^2 - P'\frac{d^2V}{dL^2} \qquad (1)$$

Here, K represents stiffness.

Assuming the polytropic process ($P' * V^{n'} = z$) inside of the muscle, equation can be written as-

$$c^{-1} = -n'\,\frac{P'+P_0}{V}\left(\frac{dV}{dL}\right)^2 - P'\frac{d^2V}{dL^2} \qquad (2)$$

Here P' is the internal pressure, V is specific volume, n' is polytropic index and z is a constant.

.

As both terms depend upon pressure, compliance (equivalent to the spring constant) can be adapted by controlling the pressure. [2]

2.1.2. Comparison of PAM's and Skeletal Muscles: [2]

PAM's resemble skeletal muscle in such a way that both are linear contractile actuators that show a decreasing load-contraction relation Fluidic actuators i.e. PAM's generate motion only in one direction. Just like skeletal muscles two actuators are needed to be coupled so that bidirectional motion can be achieved one actuator for each direction. One muscle moves the load while the other acts as brake to stop the load at desired position. To change the direction of moving load the functions of the muscles are interchanged. The antagonistic coupling can be used for linear as well as rotational motion. It can also control the joint compliance as in the skeletal muscles.

The following are the differences between the biological muscles and PAM's:

- Skeletal muscles do not change volume during contraction.
- Unlike PAM's, they have a modular structure having large number of parallel and series connections of microscopic contractile systems.
- Human muscles have internal force and strain gauges.

2.2. Classification of Air Muscles: [2]

2.2.1. Mckibben Braided Muscles:

In my research, I have studied a specific type of air muscle, the Mckibben Air Muscle, which is the most widely used type of air muscle.

2.2.1.1. Construction of Mckibben Air muscle:

The design of an Air Muscle basically consists of soft silicone rubber tube sheathed by braided nylon or polyester mesh shell with the help of mechanical fittings. One end of the air muscle is sealed while the other end is connected to pressurized air source. As the internal

.

rubber bladder is filled by the air it seeks to expand. The nylon mesh resists the rubber tube to expand along the diameter. The inherent characteristic of the nylon mesh is such that the maximum diameter of the nylon mesh increases with decrease in its length. The unique nature of the woven nylon allows the expansion of air muscle in terms of diameter tube until a certain limit. After this stage as the pressure increases the air muscle gets contracted thus decreasing its length and subsequently increasing its diameter and in turn giving more space for the expansion of the inner tube. Hence as the pressure increases net result would be such that the length of the air muscle decreases while it expands in term of the diameter. If a load is attached to the sealed end it will be displaced to the amount of the decreased length provided the load is in the operating range. This pulling action on the load when effectively utilized could provide the necessary motion. [4]

As the Mckibben muscle is pressurized by air, the rubber tube is pressed against the mesh laterally. Thus, internal pressure is balanced by the tension in the fiber of the mesh due to the curvature of the rubber tube. When the external force is applied on the air muscle it gets balanced by this axial tension which is integrated at the end points of the mesh. If the input pressure of the air is less than the threshold pressure the rubber tube gets inflated, however doesn't come in contact with outer mesh. Hence sufficient tension is not produced in the mesh, which in turn prevents the air muscle to bulge and thereby restricts the contractive movement to uplift the external force. [2]

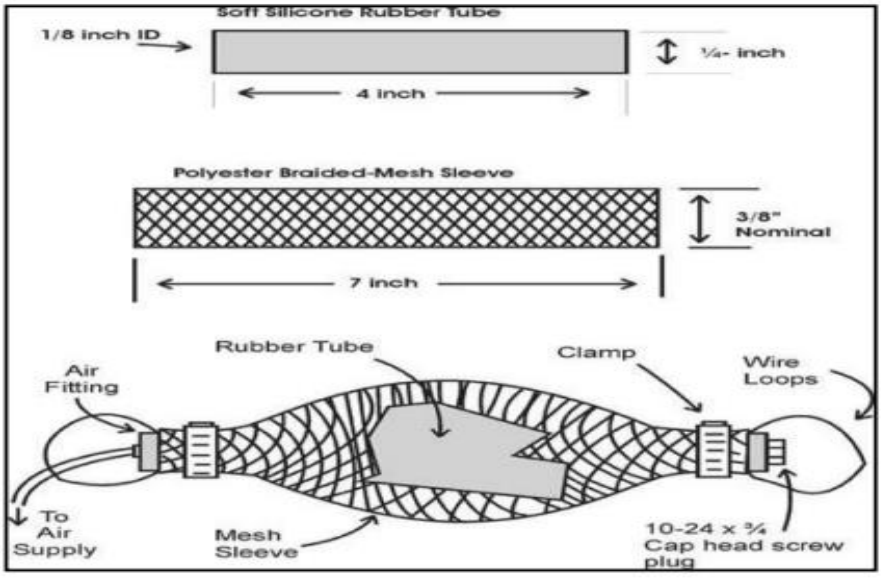

Figure 1: Construction details of Air Muscle [4]

.

There are 3 positions of air muscle respectively-

Normal, stretched and actuated length.

Figure 2: Length of Air Muscle (a): Stretched Air Muscle (of maximum length Lm). [4]

(b): Air Muscle (of length L_0) in normal state.

(c): Air Muscle (of length L) under pressure.

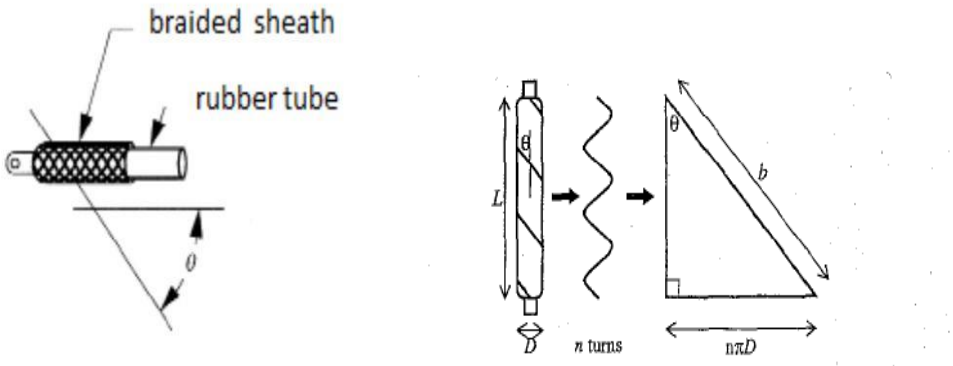

a. b.

Figure 3: Geometry of Air Muscle- Polyester braid angle (a). Geometry of actuator. Middle portion of the actuator is modeled as perfect cylinder with length *L,* diameter *D.* 0, angle between braded thread and cylinder long axis, *n,* number of turns of thread, and *b,* thread length. (b) Relationship between above parameters is illustrated by triangle. [3]

.

The typical static behavior of an air muscle can be demonstrated by an example muscle from Tondu et al. This is described here only for the purpose of showing characteristic behavior of a muscle. Following are the values mentioned by Tondu et al. [2, 11] 650 N at rest length, 300 N at 15% contraction, 0 N a 30% contraction at pressure equal to 300 kPa. Rest length equal to 150 mm, diameter = 14 mm, and weight = 50 g.

The higher the maximum pressure which muscle can withstand, the higher is the energy which can be transferred. However, as the toughness of the diaphragm i.e. the inner bladder is increased to increase the maximum pressure, its threshold pressure also increases.

Chou and Hannaford [3] have reported values of hysteresis width ranging from 0.2 cm – 0.5 cm and height varying from 5 to 10 N for a nylon braid muscle of 14 cm rest length and 1.1 cm rest diameter. The threshold pressure reported was 90 kPa.

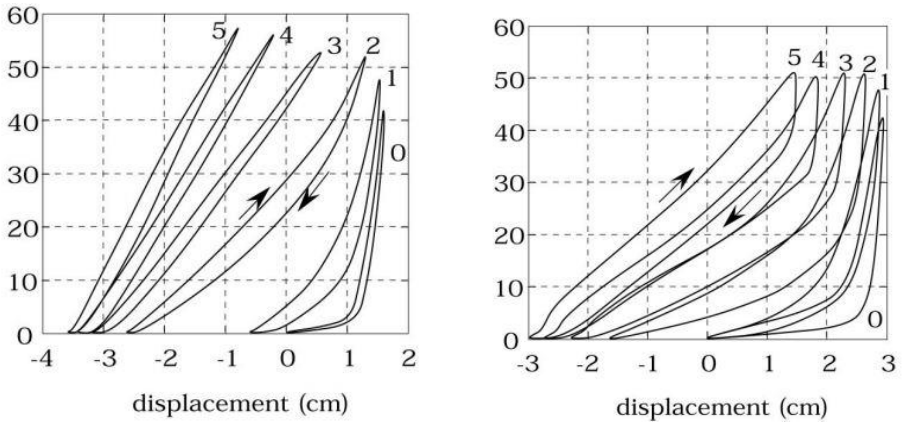

Figure 4: McKibben Muscle tension (N) and hysteresis at isobaric conditions (0, 100, 200, 300, 400 and 500 kPa), (a) Nylon braid, (b) fiberglass braid. [3]

Threshold pressure and inherent dry friction are the main disadvantages of the Mckibben muscles. Accurate position control is very difficult to achieve because dry friction causes the air muscle to become warm and they behave in a different way than cold ones [2, 13]. Also, Hesselroth et al. [2, 14] reported that positional drift of the Rubbertuator was observed when the actuator pressure was oscillating about a fixed value. Other drawback of braided muscle is that only limited displacement can be achieved by its actuation.

.

2.2.1.2. Braid Structure: [6]

The braid structure plays very important role in deciding performance characteristics and preventing over inflation. The expansion of the muscle is radial and its resulting contraction is done due the virtue of braid structure. Even the settling limit of contraction and dilation depends upon the braid structure.

The contraction of the pneumatic muscle is mostly around 30-35% (Caldwell, Medrano-Cerda and Goodwin 1995) and is given in terms of braid angle. The maximum contraction of the muscle is achieved at the inter braid angle equal to 54 degrees. The maximum diameter of the muscle or the minimum braid angle are limited by due to maximum force between adjacent strands of the braid or due to larger size of the bladder which prevents full expansion of the outer bladder. If the bladder diameter is small enough then the braid angle will depend upon weave pattern (typically a 2/2 Twill (Braidweaver 2005), material of the fiber and its diameter. The range of contraction of the muscle varies from maximum to minimum braid angle. Hence by lowering the braid angle dynamic range of the contraction can be increased.

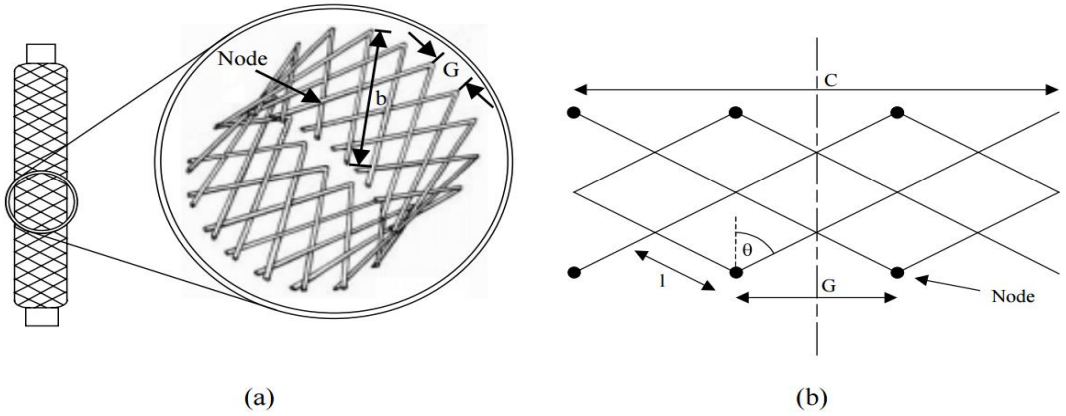

Figure 5: Braid material (a) and unrolled (b) [6]

Theoretical calculation for minimum braid angle-

Figure (a) shows a small section of braid around the air muscle's circumference is assumed to be unrolled to form a weave pattern. Figure (b) shows the axis is aligned along the length of the air muscle. The point where strands crossover is known as a node. G is the distance

.

between two nodes. C is the circumference of the air muscle and N_c is number of nodes in one circulation of the circumference. Figure (b) shows N_c=3. As per (Schulte 1962)

$$D_0 = \frac{b}{n\pi} \tag{3}$$

Therefore

$$l = \frac{\pi . D_0}{2 . N_c} \tag{4}$$

The node separation is given by

$$G = 2l \sin \theta \tag{5}$$

The structure of the braid shown in Figure assumes that there is only one strand in each path having thicknessW_b. In reality number of parallel strands follow in each path, but principle of the analysis remains the same.

$$X = Y \cos \theta \;\Rightarrow Y = \frac{W_b}{2 * \cos \theta} \tag{6}$$

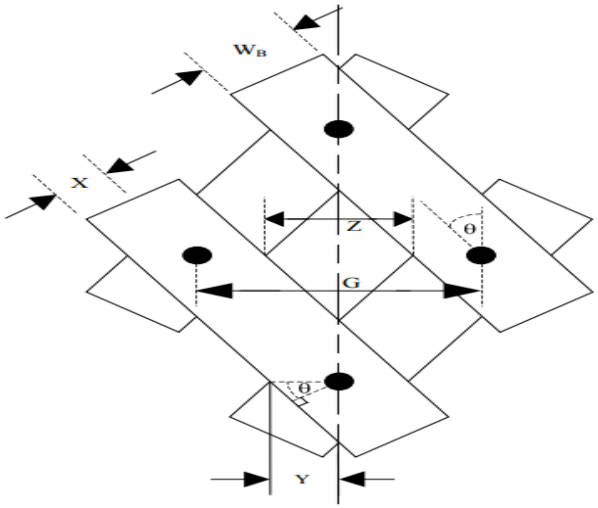

Figure 6: Braid structure assuming single strands. [6]

The minimum braid angle can be obtained when G = (2 * Y)

By substituting above relation,

.

$$\Theta_{min} = \frac{\sin^{-1}(\frac{2.W_b.N_c}{\pi D_0})}{2} \quad (7)$$

By substituting thickness in terms of diameter of one strand (D_s) and number of parallel strands (S)

$$W_b = D_s.S \quad (8)$$

Also

$$N_c = \frac{N}{2.S} \quad (9)$$

Where $N$is number of strands to create complete muscles.

Therefore, the minimum braid angle is given by

$$\Theta_{min} = \frac{\sin^{-1}(\frac{Ds.N}{\pi D_0})}{2} \quad (10)$$

This calculated angle remains constant irrespective of its length if Ds, S, and N are assumed to remain constant. Maximum dilated length can be calculated by using the equation by Schulte (1962). L_{max} is of more importance for practically design as robotic application.

Therefore

2.2.1.3. Friction/Hysteresis: [6]

$$L_{max} = b\ \cos\Theta_{min} = L_{max} = b\cos(\frac{\sin^{-1}\left(\frac{2.W_b.N_c}{\pi D_0}\right)}{2}) \quad (11)$$

Force/displacement hysteresis is observed during the operation of air muscles as discussed in Chou and Hannaford (1996) and Tondu and Lopez (2000). It is mainly due to friction between braid strands. Tondu and Lopez (2000) also pointed that even though there is contact inner bladder liner and braid does not create friction as the liner is rigidly locked to the braid on account of inner pressure. To account for the strand friction Chou and Hannaford proposed the idea of adding a constant force offset to the measured force during

.

the contraction of the muscle while subtracting it during extension. Although Tondu and Lopez further tried to quantify the offset value by modeling the friction as it was a static based model, it could not provide accurate force data (Schulte 1962; Chou and Hannaford 1996; Tsagarakis and Caldwell 2000; Davis et al. 2003). As per Tondu and Lopez (2000) a parameter K which "tunes the slope of the considered static model" is introduced to overcome the issue. Although the model is more accurate than Chou and Hannaford, it relies greatly on the experimental data.

2.2.1.4. Braid Contact Area: [6]

The braid strands rub against each other and hence friction is produced which should be included in the mathematical model. The expression for static dry friction of the braid as per Tondu and Lopez (2000) is given by-

$$F_{friction} = f_s * S_{contact} * P \quad (12)$$

Where $F_{friction}$ denotes resisting force caused by the friction, fs is the coefficient of friction (0.15 – 0.25 for a nylon and $S_{contact}$ is the contact area between the strands. Due to the weaving of the strands, contact varies according to the braid angle. Hence contact area should be calculated. One braid crossover point is taken into account to calculate the area. As per the diagram of one single braid crossover point

$$tan\theta = \frac{x}{y} \quad (13)$$

$$\sin\theta = \frac{W_B}{2y} \quad (14)$$

$$S_{one} = 2 * x * y \quad (15)$$

Area of one contact polygon S_{one} can stated as

.

$$S_{one} = \frac{{W_B}^2}{2 \sin\theta \cos\theta} \quad (16)$$

W_B is the width of the braid strand. It is assumed that a single strand fallows each path. As in the practical case number of parallel strands are used where W_B is the total width of the strands. Therefore, the total contact is given by

$$S_{contacts} = \frac{N_{contatcs}{W_B}^2}{2 \sin\theta \cos\theta} \quad (17)$$

N contacts denote total number of crossover points in the air muscle.

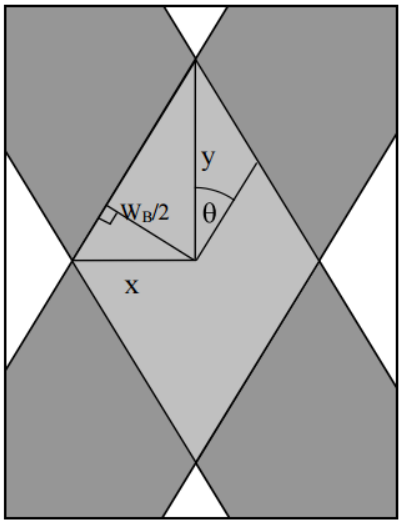

Figure 7: One single braid crossover point. [6]

When the air muscle is at maximum dilation, the braid is minimum and hence it can be assumed that the whole area of the muscle is made up of crossover points instead of experimentally calculating them.

By using length, diameter and minimum θ equations surface area can be calculated as fllows-

$$Surface\ Area = \pi * D_{min*} * L_{min} = S_{one} * N_{contacts} \quad (18)$$

By substituting above equations:

$$N_{contacts} = \frac{2*b^{2*} \sin^2\theta_{min*} \cos^2\theta_{min}}{n*{W_B}^2} \quad (19)$$

.

Therefore,

$$S_{contacts} = S_{one} * N_{contacts} \quad (20),$$

Therefore,

$$S_{contacts} = \frac{b^{2*} \sin^2 \theta_{min} * \cos^2 \theta_{min}}{n * sin\theta * cos\theta} \quad (21)$$

As a result, the frictional force can be calculated by substituting $S_{contacts}$ in equation 12.

2.2.1.5. Finite Element Modeling: [5]

The FE modeling was primarily undertaken to verify force generated due to applied load at certain pressures. Linear-static solver in educational FEA code LUSAS was used for the modeling. The PAM was considered as cylinder having orthotropic material which represent is membrane and braids accordingly.

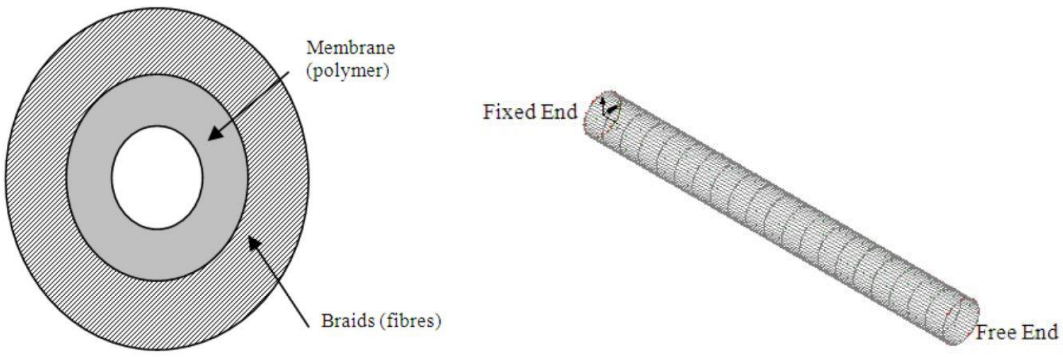

(a) (b)

Figure 8: Orthotropic material layers (a), Meshed model of a PAM (b) [5]

Other than longitudinal axis in transitional freedom, all other transitional and rotational degrees of freedom are restricted so that muscle can move only in direction. As this is set,

.

loads are increased to apply force on the PAM at the free end. By applying FE shell mesh to the structure loads and displacement is achieved in every direction along the Cartesian axis system. Relation of force with displacement was observed for certain pressures. Also, stiffness of PAM actuated with constant pressure was plotted against load applied on the PAM. Load is increased from 10 N to 100 N while the pressure is varied from 100 KPa to 500 KPa. The FE model can be modified by including nonlinear material model so that hyper elastic membrane stretching–expansion can be incorporated.

Figure 9: Linear-static FEA results [5]

(a) Fully inflated at 500 kPa (L=263.55 cm)

(b) Axial load 30 N (L = 273.83 mm)

(c) Axial load 70 N (L = 287.53 mm)

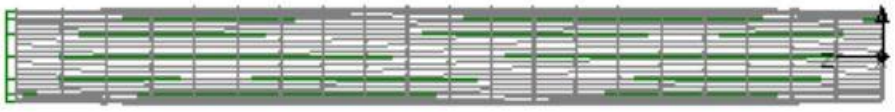

(d) Axial load 100 N (L = 297.70 mm)

.

2.2.2. Sleeve Bladder Muscle: [2]

These are different type of braided air muscles. The difference between sleeve bladder muscles is that the inner bladder is not connected to the mesh at the two ends with the help of the clamps as in the case of McKibben muscles. Here, only braid is connected to the end fitting. The advantage of these kinds of PAM's are that they are very easy to construct. A sleeved Bladder Muscle is a subject of the patent of Bullens.

2.2.3. Pleated PAM: [2]

Pleated PAM (PPAM) was developed by Daerden recently. It consists of rearranging kind of membrane having no mesh. Hence it implies that there is no material strain during the inflation of the muscle. The membrane has number of pleats along the axial direction which unfold during its expansion. The stresses in membrane are in parallel direction and are kept negligibly small.

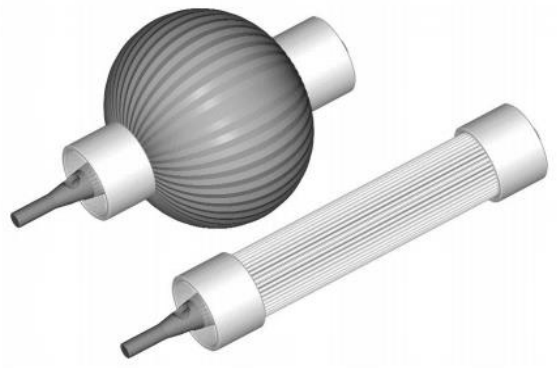

Figure 10: Pleated Muscle, fully stretched and inflated. [2]

These stresses decrease with the increase in number of pleats and hence very less energy is required to expand the membrane as compared to the other air muscles. Also, hysteresis which is a major drawback of braided muscles, is not seen in PPAM as the friction between membrane and mesh is totally absent. Very low amount of energy is lost during the bulging of the flexion of the muscle. The characteristics of the PPAM's depend upon ratio of full length to minimum diameter, strain behavior of material of the membrane, rate of contraction and the applied pressure. Contraction force can be represented with following formula:

$$F_t = \rho {L_0}^2 f_t(\varepsilon, \frac{L_0}{R_{min}}, a) \quad (22)$$

.

L_0, represents the muscles full length, R is the minimum radius, a is the dimensionless factor accounting for the elasticity of the membrane. f_t is dimensionless function which depends upon rate of contraction, geometry, and behavior of material. The factor of elasticity can be eliminated by using material having high tensile strength and stiffness.

The PPAM is very strong in comparison to other PAM's having greater linear displacement without having any hysteresis. When weight and compliance are of prime importance, use of PPAM's is ideal. Example of PPAM's in robotics are jumping, walking or running robots, grippers which can provide grip with varying firmness and flexible robot arms. As compared to braided muscles accurate positioning and controlling can be achieved easily and hence these are more suitable to fulfill above objectives.

2.2.4. Netted Muscles: [2]

The main difference between braided and netted muscles is that density of the mesh in netted muscle is higher as the mesh has large number of holes. Hence the stretching membrane in the netted mesh can withstand relatively lower pressures. So these kind of muscles usually have pleated i.e. rearranging internal bladder.

2.2.4.1. Yarlott Muscle

This is a US patented muscle developed by Yarlott. The bladder is made up of an elastomer having prolate spheroidal shape. The bladder is netted by series of strands running axially, end to end to avoid the elastic expansion of membrane. Instead of net, a single strand can be wounded helically about the shell.

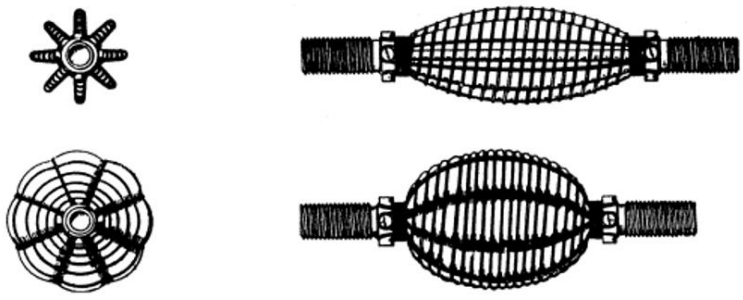

Figure 11: Yarlott Muscle. [2]

.

When the muscle is fully inflated, it looks like a spheroid. As the air is removed from the muscle the axial strands straighten to force the bladder in its shape characterized by series of ridges and valleys. The surface area of bladder does not change as the rearranging surface accounts for the expansion of the muscle. Since the stretching of the bladder is reduced in this way, more pneumatic energy is transformed into mechanical power. Though the axial strands would be fully straightened and under tremendous tension during the complete elongation, it is not yielded due to its material properties. Yarlott muscles mostly operate at low gauge pressures.

2.2.4.2. ROMAC

Robot Muscle Actuator is also a US patented muscle designed by G. Immega and M Kukoji in 1986. It has articulated polylobe bladder coupled with netting of a wire fitted end to end. The main characteristics of the bladder material used in ROMAC are its high tensile stiffness, flexibility and fluid –tightness. The netting consists of stretchable, flexible tension links which are connected at nodes forming a four-sided diamond apertures in the overall network. Similar to all muscles, the net expands radially and contracts axially and as a result the base of each protruding lobe changes. With a flexible seam two base sides of adjacent lobes are connected to each other. As the friction is absent during the expansion of membrane comparatively higher force can be achieved with negligible hysteresis in ROMAC. The standard values cited for ROMAC are muscles forces ranging from 4500 N to 13600 N at gauge pressures of 700 kPa having maximum contractions upto 50%.

.

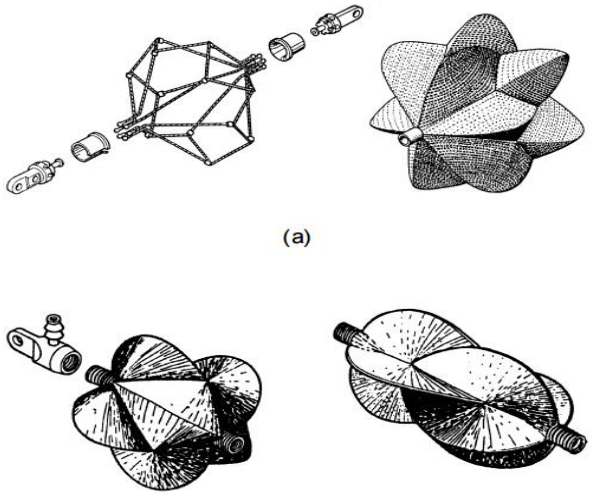

(b)

Figure 12: ROMAC, standard version (a) and miniature version (b) [2]

2.2.4.3. Kukoji Muscles

It is a variation of Mckibben muscle having open-meshed net unlike tightly woven braid. There is a gap between the membrane and the mesh during the no load condition. It disappears as the muscle is applied with high extending load. The condition of the muscle when not activated with pressure however applied with the load such that net fits the diaphragm is the fully extended condition. In these muscles as the net contracts at a higher rate than membrane, to avoid the buckling at the ends initial gap is provided.

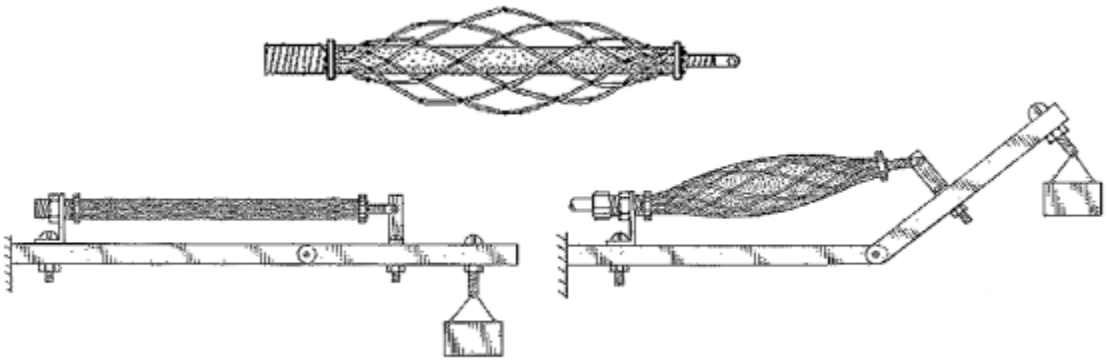

Figure 13: Kukolj Muscle. [2]

.

The figure shows the muscle in different cases like uninflated, fully elongated and actuated to pick up the load respectively.

2.2.5. Embedded Muscles

The following are different kinds of embedded muscles:

2.2.5.1. Morin Muscle

In this muscle, rubber tube is embedded by high tensile stiffness threads made up of cotton, rayon, steel or asbestos which run along the actuators axis or along a double helix path. The two-phase membrane is attached between to clamps so that the muscle can be sealed and applied with load. The tension is balanced by the fibers while the rubber bladder gets inflated during contraction. In this muscle, rubber tube is embedded by high tensile stiffness threads made up of cotton, rayon, steel or asbestos which run along the actuators axis or along a double helix path. The two-phase membrane is attached between to clamps so that the muscle can be sealed and applied with load. The tension is balanced by the fibers while the rubber bladder gets inflated during contraction. Various fluids can be used with Morin muscles such as air, oil, steam and water. There are three patented designs described by Morin which are namely, a. overpressure design b. under-pressure design and c. concentric membrane design.

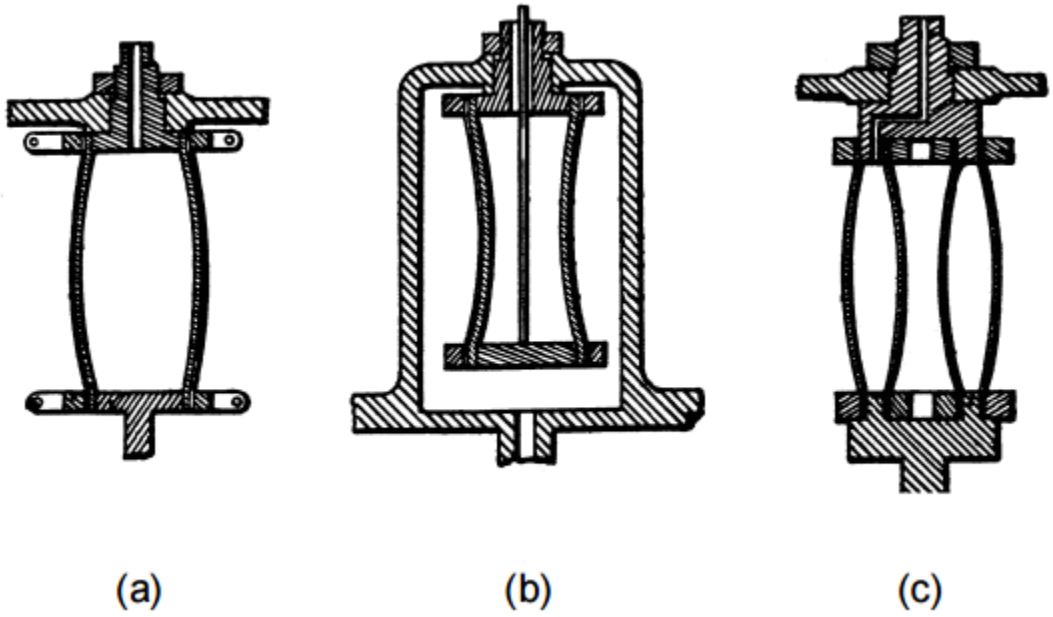

.

Figure 14: Morin Muscle Designs [2]

2.2.5.2. Baldwin Muscle

It basically follows the design of Morin muscles. The elastomeric membrane is embedded by glass filaments along the vertical axis. The so formed membrane has very high modulus of elasticity along the direction filaments as compared to direction perpendicular to it. As discussed earlier as there is no friction with outer mesh, the muscle has very less hysteresis. Also, the threshold pressure is very low. As radial expansion is high the pressure is limited to 100 kPa. As per Baldwin 1600 N force can be lifted by the muscle. Life tests indicate operating life of 10000 to 30000 cycles when a weight of 45 kg was alternatingly lifted and lowered at about 100 kPa.

2.3. Existing Theoretical Model to Derive Equation of Force: [3]

The Static Physical model of Mckibben Muscles derived by Chou and Hannaford which give us the formula for force applied on the air muscles is studied in this section. [3]

Work input done on the Mckibben Muscle as the pressurized air inflates the air muscle is given by

$$dW_{in} = \int_{S_i}(P - P_0)dl_i.dS_i = (P - P_0)\int_{s_i} dl_i.dS_i = P'dV \qquad (23)$$

The output work is associated with volume change as the actuator shortens is given by

$$dW_{out} = -Fdl \qquad (24)$$

As per the law of conservation

$$dW_{out} = dW_{in} \qquad (25)$$

$$-Fdl = P'dV \qquad (26)$$

.

$$-Fdl = P'dV \tag{27}$$

$$F = -P\frac{dV}{dL} \tag{28}$$

Assumptions:

The extensibility of shell threads is very low; volume of the air muscle depends on its length.

The middle portion of the air muscle is assumed to be a perfect cylinder having L and D as the length and diameter of the cylinder.

$$L = b\ cos\theta \tag{29}$$

$$D = b\ \frac{\sin\theta}{n\pi} \tag{30}$$

Therefore, the volume is

$$V = \frac{1}{4}\pi D^2 L \tag{31}$$

$$V = \frac{b^3}{4\pi n^2} sin^2\theta cos\theta \tag{32}$$

$$F = -P'\frac{dV/d\theta}{dL/d\theta} \tag{33}$$

Therefore

$$F = \frac{\pi {D_0}^2 P'}{4}(3cos^2\theta - 1) \tag{34}$$

$D_0 = b/\pi n$ is the diameter when θ is equal to 90 degrees.

The tension is thus linearly proportional to the pressure and is a monotonic function of the braid angle. If force applied (F) on the muscle is equal to zero in equation (34), θ is 54.7 degrees. Hence, the maximum shortening will be reached at θ is 54.7 degrees.

.

Effect of thickness of the nylon shell and the bladder on the length of the air muscle [3]:

When the thickness (t_k) of the shell and the bladder is considered, the volume can be expressed as follows:

$$V = \frac{1}{4}\pi(D - 2t_k)^2 L \tag{35}$$

Therefore, the formula for the force developed by the air muscle can be given by

$$F = \frac{\pi {D_0}^2 P'}{4}(3cos^2\theta - 1) + \pi P'[D_0 * t_k\left(2 * sin\theta - \frac{1}{sin\theta}\right) - t_k^2] \tag{36}$$

This equation gives more accurate results as compared to equation (34). However, thickness, t_k, is often neglected in order to find the change in length.

2.4. Existing Experimental Model to Measure Contraction of Air Muscles at Varying loads: [4]

"Theoretical and Experimental Modeling of Air Muscle" [4] paper is discussed in this section. It describes testing of air muscles to measure the contraction of the air muscles at different loads. Effect of varying pressures was also taken into account during the experiment. The relationship between volume and variation of pressures at different loads is also analyzed. The experimental setup included a compressed air supply, air muscles, a pressure regulator, 0.5 kg weights, and a travelling microscope to measure the length contraction. Pressurized air was induced in the air muscle, and the contraction of the air muscle was observed for the respective loads.

The graph of variation of contraction of the air muscle with variation of pressure at different loads concludes that as the pressure increases, the contraction in length of the air muscle increases. Then, as the load decreases, the contraction in length increases. Also, I have compared my theoretical plot of contraction vs. pressure with this published plot. We can see that both plots have similarly shaped curves, which proves that my theoretical model is correct. Theoretical model is explained in forthcoming chapter. The range for contraction is about 2 mm to 30 mm in my model as against 5 mm to 45 mm in this published paper [4].

.

The pressure increase from 30 psi to 80 psi is similar to te pressure increase mentioned in the paper, as well.

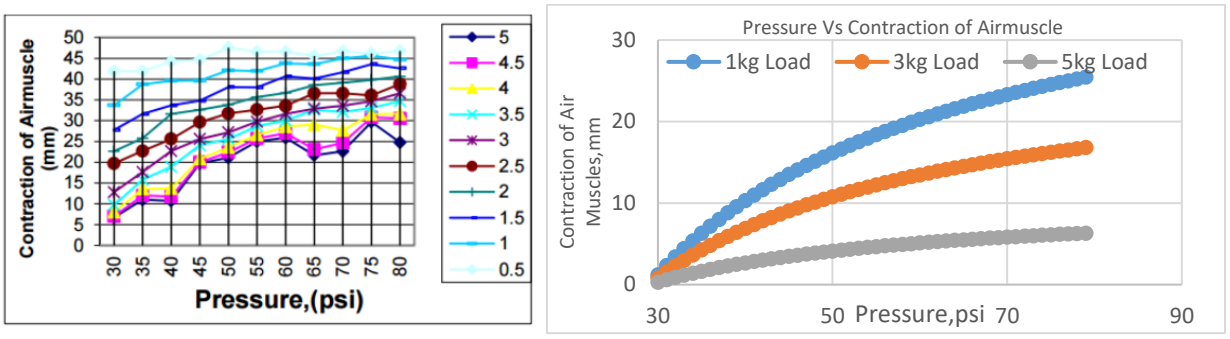

a. b.

Figure 15: Comparison of Contraction of Air Muscles vs. Pressure Plots [4]

For the second test, volume trapped in the muscle was plotted against varying pressures at different loads. It was observed as the pressure increases in steps, the volume increases and the contracted length decreases for a constant load.

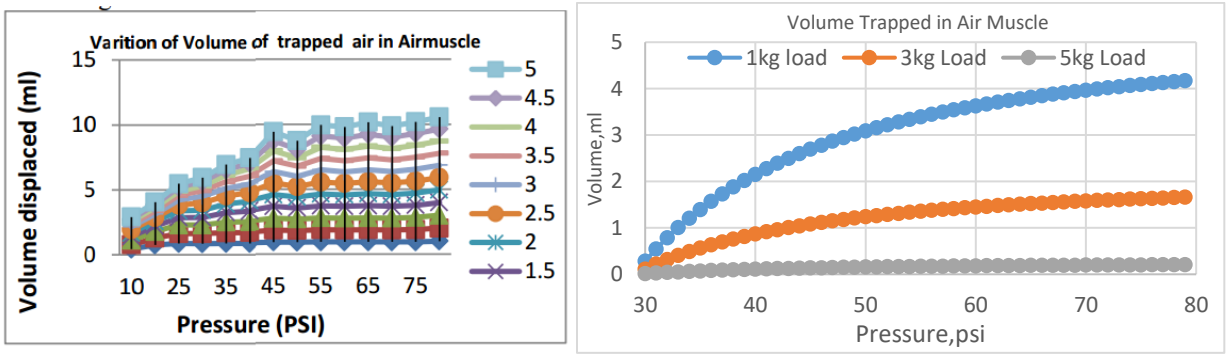

Figure 16: Comparison of Volume Trapped vs. Pressure Plots [4]

Similarly, I have also plotted the graph of volume trapped vs. pressure, and again the trending curves are similar to those in the published plot. Volume displaced during contraction was in the range of 0–5 ml as compared to the 0–11 ml range in the published plot. Once again pressure was increased from 30 to 80 psi. The only difference between these two plots is that my theoretically modeled plot shows the least volume displaced for the highest load, while the published plot has the highest volume displaced for the highest load. As the load applied to the air muscle increases, the contraction will be less, as the load acts against the direction of contraction. The figures in this paper demonstrate that as the

.

load (i.e., applied force) is increased, the corresponding volume decreases. The error in the paper can be because of the experimental error while performing the same.

Following are the observations of the experiments mentioned in the published paper.

For Pressure, P = constant

$F1 > F2 > F3$

$v1 < v2 < v3$

$x1 > x2 > x3$

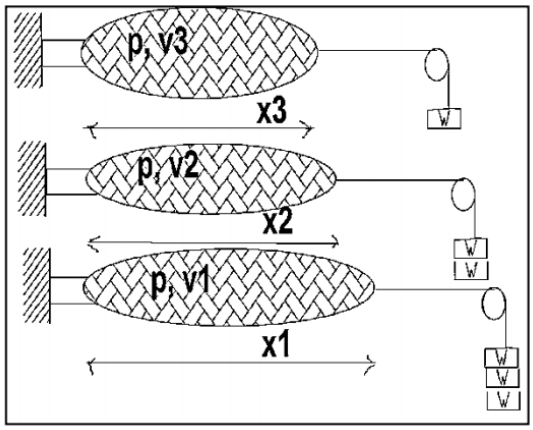

Figure 17: Behavior of Air Muscle at constant pressure. [4]

For force, F = constant

$p1 < p2 < p3 < p4$

$v1 < v2 < v3 < v4$

$x1 > x2 > x3 > x4$

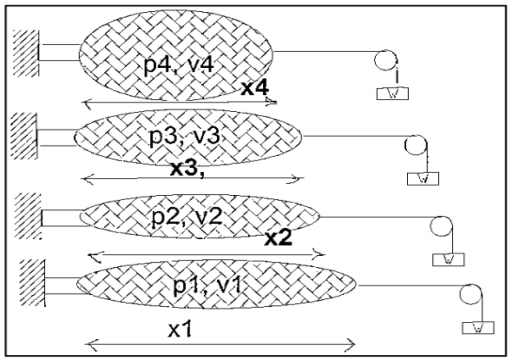

.

Figure 18: Operation of Air Muscle at constant load. [4]

Also, if the pressure is kept constant and the load increases in steps, the contraction in length and the volume decrease.

The paper also discusses a formula for the length of an inflated air muscle in the following form:

$$L = \sqrt{\frac{(b^2 - (4 * F * \pi * n^2)/P)}{3}} \tag{37}$$

As per the formula above, the length of the air muscle will increase as the pressure increases. However, as per the basic characteristic of the air muscle, the length of the air muscle should decrease as pressurized air is induced in the air muscle. The reason for this discrepancy is that Ranjan et al. has incorrectly considered output work equal to positive product of force (F) and change in length (*dl*) while deriving the equation for force applied on the air muscle.

However, the output work is associated with volume change as the actuator shortens and hence is given by:

$$dW_{out} = -Fdl \tag{24}$$

Also, the input work is given by (23)

$$dW_{in} = \int_{S_i} (P - P_0) dl_i . dS_i = (P - P_0) \int_{s_i} dl_i . dS_i = P' dV$$

And hence, the force developed in the equation should be negative times the product of pressure and change in volume. (28)

$$F = -(P * \frac{dV}{dL})$$

Therefore, the error is incorporated in the final equation of length.

Hence, the correct formula should be,

$$L = \sqrt{\frac{(b^2 + (4 * F * \pi * n^2)/P)}{3}} \tag{38}$$

.

3. Experimental Model to Test Velocity of Contraction of Air Muscles at varying Forces:

3.1. Design and Building of the Experiment Test rig

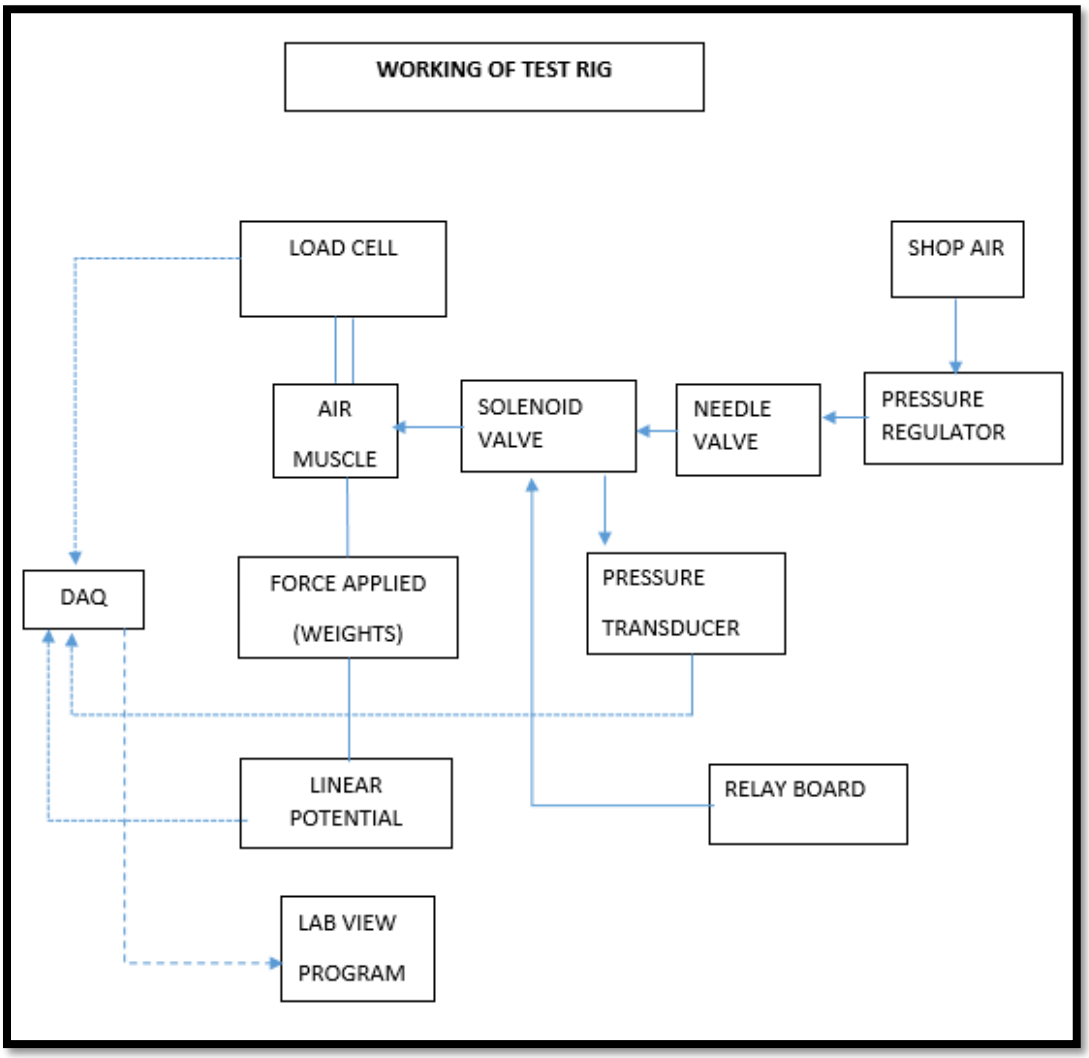

Figure 19: Block Diagram of Working of Test Rig.

An experimental test rig was designed such that an air muscle could be attached along the longitudinal axis. The two side arms of the frame were about 15 cm from each other, accommodating the lead screw arrangement which allowed the bulging of even the longest of the air muscles without any obstruction. The open end of the air muscle was attached to

.

a T-shaped valve, which was fixed to the load cell. The load cell in turn was attached to the C-shaped bracket, which was fixed to the front plate. The front plate was connected to the 30 cm-long lead screw arrangement from the back side. This arrangement helped to adjust the position of the air muscle along the longitudinal axis. This adjustment was important to accommodate weights at the bottom of the air muscle and to position the linear potentiometer below the air muscle along the longitudinal axis. A course adjustment was provided so that the lead screw could be moved along the vertical axis in order to accommodate air muscles of various sizes, including bigger air muscles having varied lengths. The whole assembly rested on a base plate. A hook was attached to the base plate to hold the linear potentiometer in a straight position.

3.2. Working of the Test Rig:

The pressure regulator regulated the pressure of the shop air flowing to the solenoid valve. A needle valve was placed in the system between the pressure regulator and the solenoid valve. The needle valve was used to control the volume flow rate of air passing in the air muscle. The volume flow rate was not measured, but readings were taken at two different volume flow rates, specified as restrictions R1 and R2, governed by position of the needle valve. R1 represents fully opened needle valve while R2 represents partially opened needle valve such that R1 is greater than R2. From the needle valve, pressurized air is passed to the pressure transducer and the 5/2 solenoid valve. From the 5/2 solenoid valve air is passed to the air muscle. Hence, the pressure transducer measured the pressure equivalent inside the air muscle. As the air muscle is actuated it is contracted along the length and load attached to it is lifted. The main parameters that were monitored during the tests were load, pressure, and the linear displacement. The linear displacement was measured with the help of linear potentiometer which was attached to the base plate, as mentioned earlier. The force applied by the air muscle when actuated (i.e., when the load was attached to it) was measured directly as the known weights were placed in the tray.

.

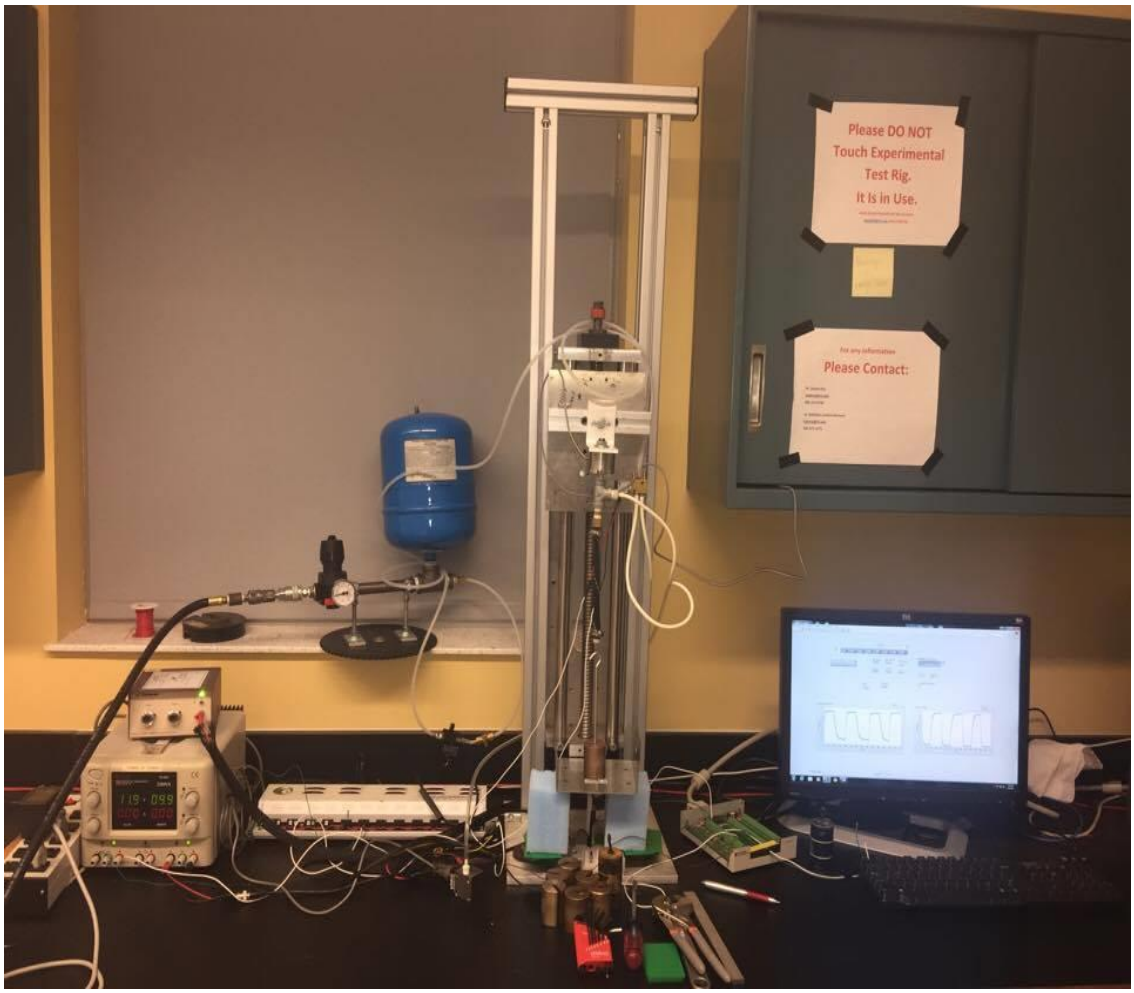

Figure 20**: Experimental Test Rig**

3.2.1. Data Acquisition

The two sensors—namely the pressure transducer and linear potentiometer—are connected to SCB - 68 NI DAQ board. The DAQ in turn was connected to the computer with the help of a data cord so that it can communicate with LabVIEW 2012, which was installed on the computer. The LabVIEW program displayed following two graphs on the front panel:

3.2.1.1. Pressure vs. Time Plot

Pressure was measured with the help of pressure transducer and the data was processed such that pressure vs. time plot was displayed on the front panel of the

.

LabVIEW program. Pressure was calibrated in psi, and time was represented in time. The linear equation used for the calibration of the pressure voltage into grams was (Y= 14.4 * X – 16.8). The equation was substituted in the block diagram of the program. The equation was found by increasing pressures incrementally from 30 to 80 psi with the help of the regulator, and the raw corresponding voltages were noted with help of the pressure transducer. The graph of voltage vs. real pressure was plotted, and the trade line equation was used for calibration. Real time pressure as well as raw pressure voltage were displayed on the panel.

Specifications:

Min voltage = +5volts
Max voltage = -5volts
The signal from the pressure transducer was amplified and conditioned, and then the output was connected to AI channel 1 of DAQ board.

3.2.1.2. Displacement vs time Plot

The displacement voltage was measured with the help of linear potentiometer and the data was processed such that displacement voltage vs. time graph was displayed on the panel. Also, real time voltage was displayed in a window.
Displacement voltage was directly converted into real displacement during the actual calculations by using the similar calibration technique like pressure. Displacement was then converted into velocity by using the slope of the displacement vs. time graph.
Specifications:
Min voltage = +5volts
Max voltage = -5volts
The signal from the linear potentiometer was connected to AI channel 5 of DAQ board. Also, the time, given in seconds, was displayed on the front panel along with the count of the number of readings taken during one test.
Specifications:
Terminal Configuration: Differential

.

Acquisition Mode: Continuous samples

Samples to Read: 100

Rate: 1000Hz

The 12V solenoid valve, which was used to actuate the air muscle, was operated by a Measurement computing relay board. The relay board was operated with the help of the LabVIEW program. A special inbuilt program was used to communicate between the relay board and the LabVIEW program. With the help of this program, seven relays could be turned on by pressing the corresponding seven buttons on the front panel. One of the buttons was used to operate the solenoid valve.

3.2.2. Analysis of Readings:

With the help of linear potentiometer readings saved in the Excel file, actual position displacement is measured by considering the voltage scale of the potentiometer. As the displacement is plotted against time, actual velocity is measured by finding the slope of the graph. From the velocity readings, maximum velocity and average velocity are measured for one of the contraction cycles observed by the air muscle. This process is carried out for the different sets of loads, pressures, and volume flow rates (restrictions) mentioned above. Sets of each type of velocity are plotted against forces ranging from 0–60N at three different pressures, namely 20 psi, 40 psi and 60 psi.

3.2.3. Example of Analysis of raw Data

In the figure 21. below, displacement of the air muscle (A1) is plotted against the time. With the help of the linear potentiometer, displacement of the of air muscle was noted at each time step. The data was recorded with help of the SQ DAQ in Lab View. The range of the linear potentiometer used in the experiment was 1 in. Initially, the linear potentiometer reads 0.8 in. As the pressure is increased to 40 psi, it can be seen that at 1 s the potentiometer reading is 0.22 in. Hence it can be understood that in 1 second, the air muscle has contracted by 0.58 in. These measurements were taken at 10 N force condition, and the volume flow rate was set to restriction R1.

.

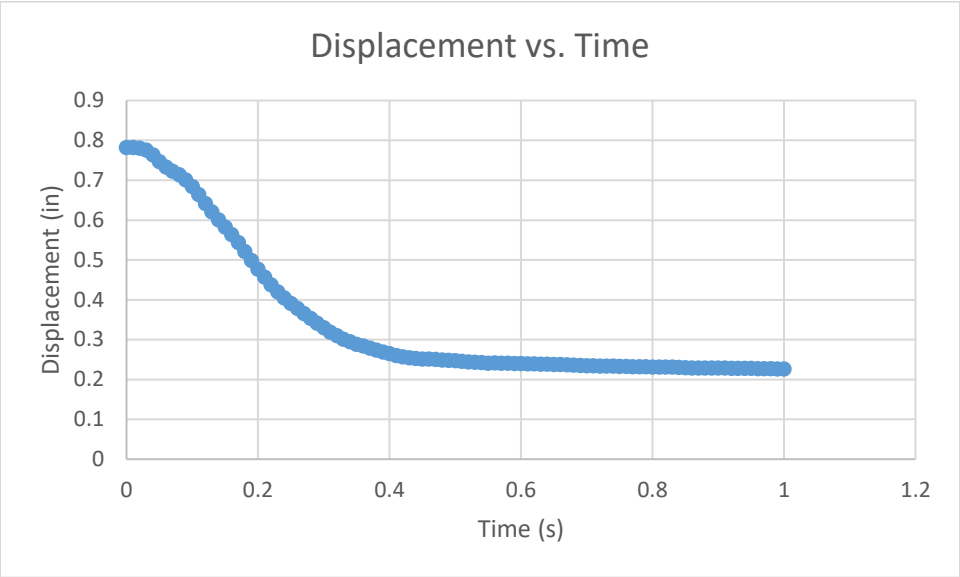

Figure 21: Displacement vs. time plot of experimental data.

In the figure 22., velocity of the contraction of air muscle is plotted against the time. With the help of displacement measurements at each time, velocity was measured. As demonstrated by the graph, velocity increases initially until a certain time and then it decreases gradually. The maximum velocity in this case is 2.251 in/s, which is measured by finding the maximum value amongst all the velocities in the time span of this contraction cycle. Similarly, the average velocity is found by measuring the average of the velocities at each step. In the Results section, maximum and average velocities at different conditions are compared to find the relationship between the velocity of contraction and force applied as a function of pressure and volume flow rate.

.

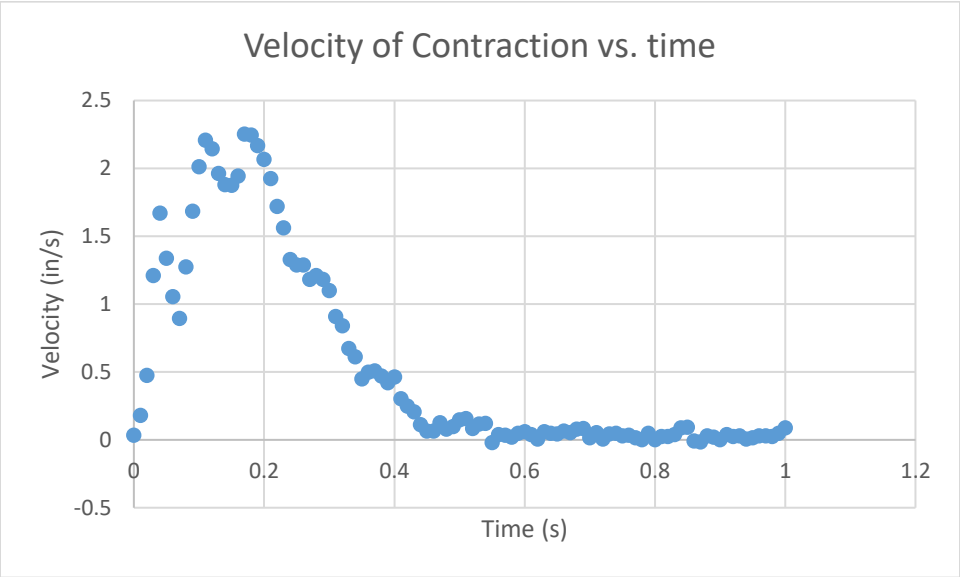

Figure 22: Velocity of contraction vs. time plot at 10 N, V1

3.3. Results:

Specifications of the air muscles used for the experiment are as follows:

	A1 (L, D) (Nominal)	A2 (L/2, D)	A3 (L, D/2)
Length (L), in	5	2.5	5
Diameter (D), in	0.375	0.375	0.1875

The thickness of all the three air muscles was 0.125 in. All of the air muscles were made from the same material.

The experiments were carried out at following two volume flow rate conditions:

R1 = volume flow rate set to restriction R1, i.e., full flow of air through needle valve

.

R2 = volume flow rate set to restriction R2, i.e., partial flow of air through needle valve

The different force conditions at which tests were carried out were as follows:

1. 0N, 2. 10 N, 3. 15N, 4. 25N, 5. 35N, 6. 50N, 7. 60N

In my thesis, similar measurements have been taken at different forces ranging from 0 to 60 N. However, for better understanding of comparison the three air muscles, unloaded and 10 N force condition is discussed in this section.

In the bar chart shown in figure 23. maximum velocities of the three air muscles (A1, A2, and A3) have been compared with each other. All the readings are taken at 20 psi gauge pressure. The X axis represents maximum velocity, while the Y axis represents the force applied on the air muscles. The first two sets are plotted for no load condition, while the next two sets are plotted when 10 N force is applied. The first and third sets are measured at volume flow rate equal to restriction R1, while the second and fourth sets are measured at volume flow rate equal to restriction R2.

The first two sets show that as the volume flow rate is reduced, the velocities decrease by more than half. The maximum velocity for A1 at no load and R1 condition is 0.8008 in/s, while it is 0.2198 in/s at R2 condition. A similar trend can be observed for A2 and A3.

Additionally, as observed in sets one and three, as the force applied on the air muscle increases, the velocity of contraction decreases. In the case of air muscle A2, the maximum velocity of contraction achieved at no load condition is 0.2637 in/s while at 10 N force, the velocity measured is 0.2001 in/s.

Lastly, it can be observed that air muscle A1 has the highest maximum velocity of contraction as compared to air muscles, A2 and A3.

.

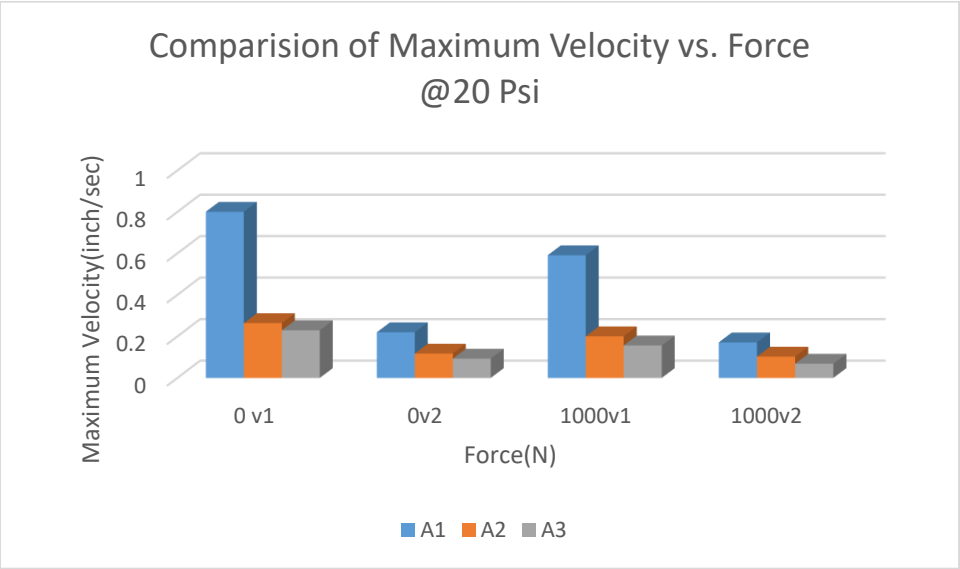

Figure 23: Comparison of maximum velocities of A1, A2 and A3 at 20 psi at 0N and 10 N load conditions, measured at both the volume flow rates (R1 and R2).

Now we will compare all the three air muscles by taking into account all the force conditions at which the air muscles were tested. Once again, the following results were obtained for restrictions R1 and R2 and at 20 psi gauge pressure.

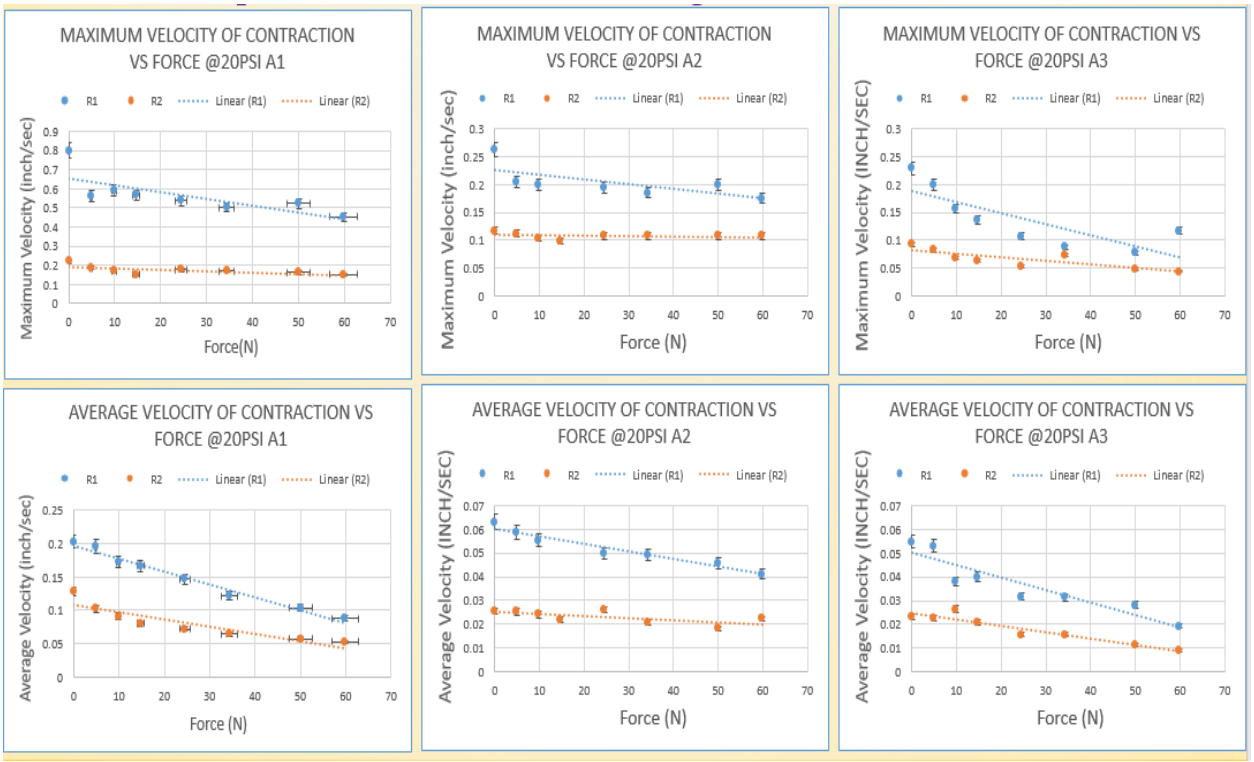

Figure 24: Comparison of maximum and average velocities of A1, A2, A3 at 20 psi at R1, R2.

.

The top three graphs in the figure 24. compare the maximum velocities against the force applied on the air muscles, while the bottom three graphs compare the average velocities against the respective forces. The blue line represents velocities measured at volume flow rate R1, while the orange line indicates the velocities measured at R2.

Similar to above bar chart, it can be observed in all the plots that as the force applied on air muscle is increased, the velocity of contraction decreases linearly. It can also be seen that for a constant force, velocity of contraction decreases if the volume flow rate is reduced.

In all the force conditions at 20 psi gauge pressure, the maximum and average velocities of air muscles A2 and A3 drop by nearly half when compared to A1. This means that if the diameter is reduced by half and the length is kept constant (or vice versa), it affects the velocity of contraction substantially. For example, the average velocity at no load and R1 condition for A1 is around 0.1 in/s, while it is about 0.06 in/s and 0.055 in/s for A2 and A3, respectively. However, for maximum load condition (i.e., 60 N force), the average velocity at R1 for A1 is around 0.8 in/s, while for A2 it is 0.04 in/s and for A3 it is 0.02 in/s. This result indicates that, at lower pressures, reduction in diameter has more effect than reduction in length as in the case of A2.

The bar chart in the figure 25. compares maximum velocities of the three air muscles at 40 psi gauge pressure. Once again, the first two sets are plotted for no load condition, while the next two sets are plotted when 10 N force is applied. The first and third sets are measured at volume flow rate equal to restriction R1, while the second and fourth sets are measured at volume flow rate equal to R2.

Here, as the volume flow rate is reduced, the velocities decrease substantially. The maximum velocity for A1 at no load and R1 restriction is 2.6904 in/s, while it is just 0.7715 in/s at R2 restriction. A2 and A3 follow a similar trend. This reduction in the maximum velocities, about 0.2 in/s, is much higher than the reduction achieved under 20 psi gauge pressure. Hence, as the pressure increases, the reduction in volume flow rate more significant affects the velocity of contraction.

Furthermore, the maximum velocities in these four sets are higher than the corresponding maximum velocities achieved under 20 psi pressure. For example, at 40 psi, the maximum velocity of contraction of the air muscle A1 at no load, restriction R1 is 2.6904 in/s, while at

.

20 psi, the same air muscle under the same conditions contracts at a velocity of just 0.5713 in/s. This clearly infers that as the pressure is increased, the velocity of contraction increases.

Similar to the results observed under 20 psi, sets one and three show that as the force applied on an air muscle is increased, velocity of contraction decreases. For instance, in the case of air muscle A3, the maximum velocity of contraction achieved at no load condition is 2.3291 in/s, while at 10 N force, the velocity is 0.9033 in/s. Also, as with previous results under varying conditions, air muscle A1 has the highest maximum velocity of contraction as compared to air muscles, A2 and A3.

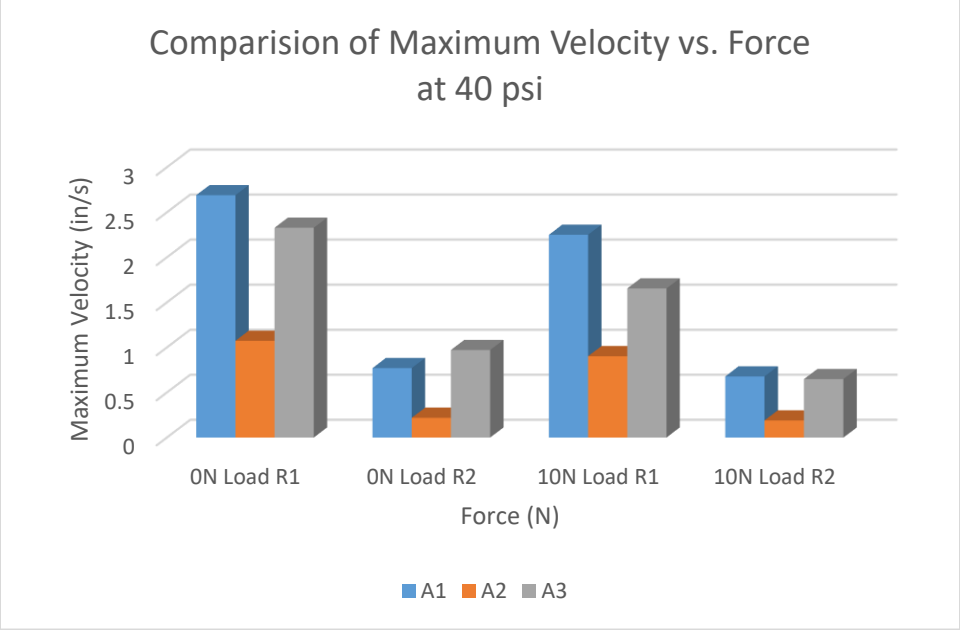

Figure 25: Comparison of maximum velocities of A1, A2 and A3 at 40 psi at 0N and 10 N load conditions, measured at both the volume flow rates (R1 and R2).

Similar to the 20 psi plots, we can compare all three air muscles at 40 psi gauge pressure by taking into account the different force conditions under which they were tested.

.

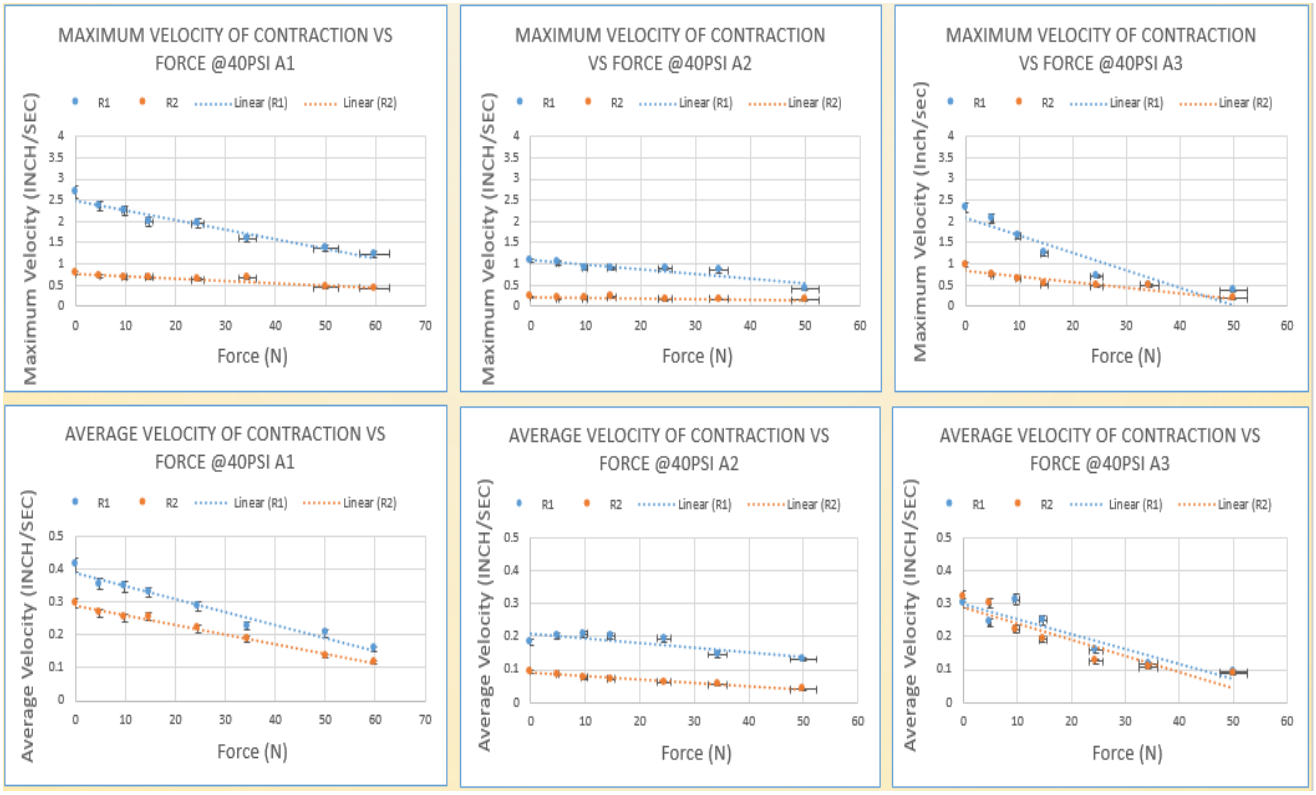

Figure 26: Comparison of maximum and average velocities of A1, A2, and A3 at 40 psi at R1, R2

The top three graphs in the figure 26. compare the maximum velocities against the force applied on the air muscles, while the bottom three graphs compare the average velocities against the respective forces. As with the 20 psi plots, the blue line represents velocities measured at volume flow rate R1, while the orange line indicates the velocities measured at R2.

Similar to the 40 psi bar chart results, all the plots show that as the force applied on the air muscle is increased, the velocity of contraction decreases linearly. It can also be seen that for a constant force, velocity of contraction decreases if the volume flow rate is reduced.

In all the force conditions at 40 psi gauge pressure, the maximum as well as average velocities of air muscle A2 (i.e., the air muscle with reduced length) are half of those of A1. However, as the pressure is increased to 40 psi, the velocity of A3 (i.e., the air muscle with reduced diameter) does not fall that much as compared to A1. For example, the average velocity at no load and R1 condition for A1 is about 0.42 in/s while the average velocity for A2 at same conditions has nearly dropped to half (i.e., around 0.2 in/s). However, the average velocity at the same conditions for A3 only decreases by about a quarter (i.e., 0.3 in/s).

.

Hence, as the pressure increases, the effect of reduction of length (A2) is greater as compared to reduction in diameter (A3).

In the bar chart shown in figure 27. maximum velocities of only two air muscles, A1 and A2, at 60 psi gauge pressure are compared with each other. Air muscle A3 is not included in 60 psi results because the contraction of this muscle was greater than the range of the linear potentiometer. Consequently, corresponding velocities could not be measured.

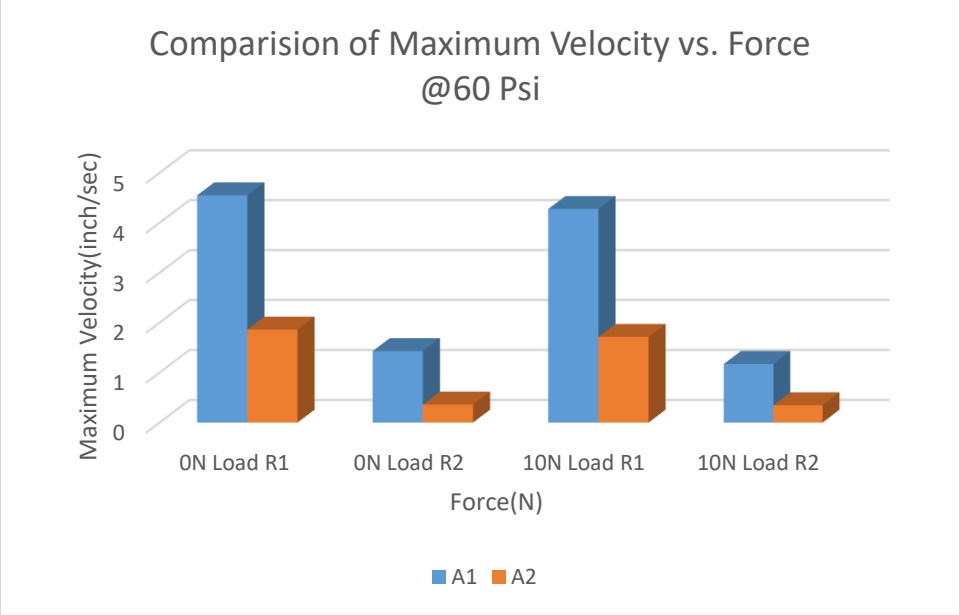

Figure 27: Comparison of maximum velocities of A1 and A2 at 60 psi at 0N and 10 N load conditions measured at both the volume flow rates (R1 and R2).

Once again, it can be seen that as the volume flow rate is reduced, the velocities decrease more drastically. The maximum velocity for A1 at no load and R1 condition is 4.5508 in/s, while it is just 1.8603 in/s at R2 restriction. A similar trend can be observed for A2. The reduction in maximum velocity of contraction is almost two-and-half times. This demonstrates that as the pressure increases, the effect of reduction in volume flow rate is greater on the velocity of contraction.

It can also be observed that the maximum velocities in all these four sets are higher than the corresponding maximum velocities in the cases of 20 and 40 psi pressure. For example, the maximum velocity of contraction of the air muscle A1 at no load, restriction R1, and 60 psi condition is 4.5508 in/s, which greater than the 20 psi and 40 psi results for the same air

.

muscle at the same load. Hence, once again it can be inferred that as the pressure increases, the velocity of contraction increases.

By observing sets one and three, it can be understood that as the force applied on the air muscle is increased, velocity of contraction decreases. This result is similar to 20 and 40 psi results. For instance, in the case of air muscle A2, the maximum velocity of contraction achieved at no load and R2 condition is 0.3613 in/s, while at 10 N force and R2 condition, the same air muscle contracts by a velocity equal to 0.3467 in/s.

It can be clearly understood that the maximum velocities of contraction of A2 are lower than A1, which has double the length as compared to A2.

At this point I would like to discuss the effect of initial length and initial diameter on the total length of the contraction (Delta L).

Length of air muscle is given by the following formula:

$$L = \left(\sqrt{\frac{\frac{4F}{\pi {D_0}^2 P'} + 1}{3}} \right) * b \qquad (39)$$

Therefore, we can say that L α (F, b/D_0^2, P').

However, Delta L = (L_0 −L).

Hence, Delta L α [L_0 - (F, b/D_0^2, P')].

From these equations, it is clear that Delta L (i.e., total length of contraction) is proportional to initial length and initial diameter. However, as there are other factors like force, pressure, and length of the thread, exact relation is not developed in my study.

Now we will see the comparison of two air muscles, A1 and A2, at 60 psi gauge pressure by taking into account all the force conditions at which the air muscles were tested. The results were obtained for both restrictions R1 and R2.

Similar to 20 and 40 psi plots, the following graphs in the figure 28. compare A1 and A2 at 60 psi gauge pressure. Like the 60 psi bar chart results, these plots show that as the force applied on the air muscle is increased, the velocity of contraction decreases linearly. Also,

.

these plots reveal that for a constant force, velocity of contraction decreases if the volume flow rate is reduced. In all the force conditions, the maximum as well as average velocities for A1 are nearly double those of A2.

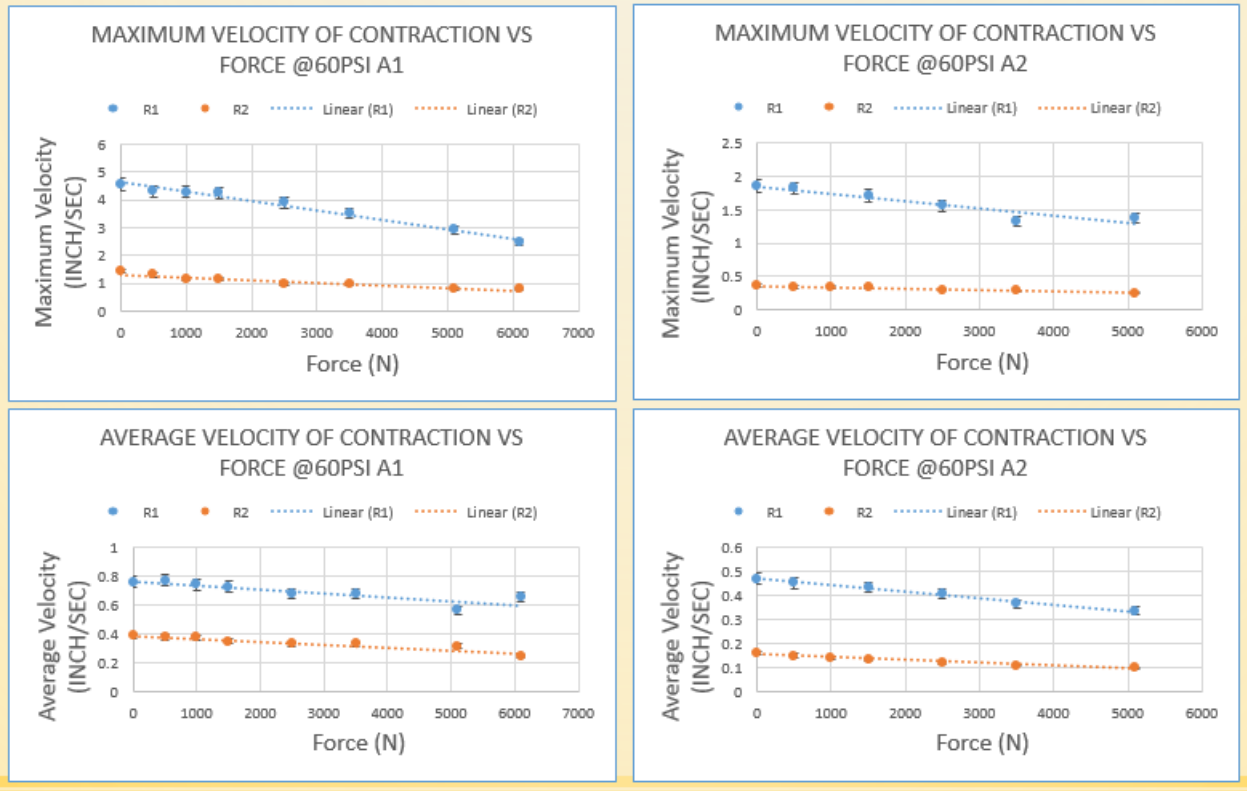

Figure 28: Comparison of maximum and average velocities of A1 and A2 at 60 psi at R1, R2.

In the last part of the results, Delta L (i.e., the total length or maximum length of contraction of the air muscles) is discussed. The following graphs address the change in Delta L due to the force applied on the air muscles. The X-axis represents Delta L and the Y-axis represents force (N). All three graphs shown in figure 29. are plotted for the same air muscle, A1. In the first graph, Delta L is plotted against force at gauge pressure equal to 20 psi. The second and third graphs are plotted for the pressures equal to 40 psi and 60 psi, respectively. In all cases, the blue line represents the measurements taken at volume flow rate R1, and the orange line represents measurements taken at volume flow rate R2. First, in all cases, as the force applied on the air muscles is increased, length of contraction (i.e., Delta L) decreases. For example, the maximum contraction for A1 at no load, R1, and 20 psi condition is about 0.16 in, while the same air muscle contracts only about 0.06 in when the force is increased to 60 N.

.

Second, as the pressure is increased, as in the case of second and third graph, the length of contraction for corresponding force is also increased. As with the no load condition, Delta L is at its maximum (around 0.9 in) at 60 psi, while at 40 psi it drops to 0.6 in, and at 20 psi it drops even further, to just 0.16 in.

One important observation to make here is that at all the three pressure conditions, Delta L remains nearly the same even though the volume flow rate is reduced to restriction R2. Therefore, it can be inferred that the reduction in velocity due to reduction in volume flow rate is only due to the time factor involved in it.

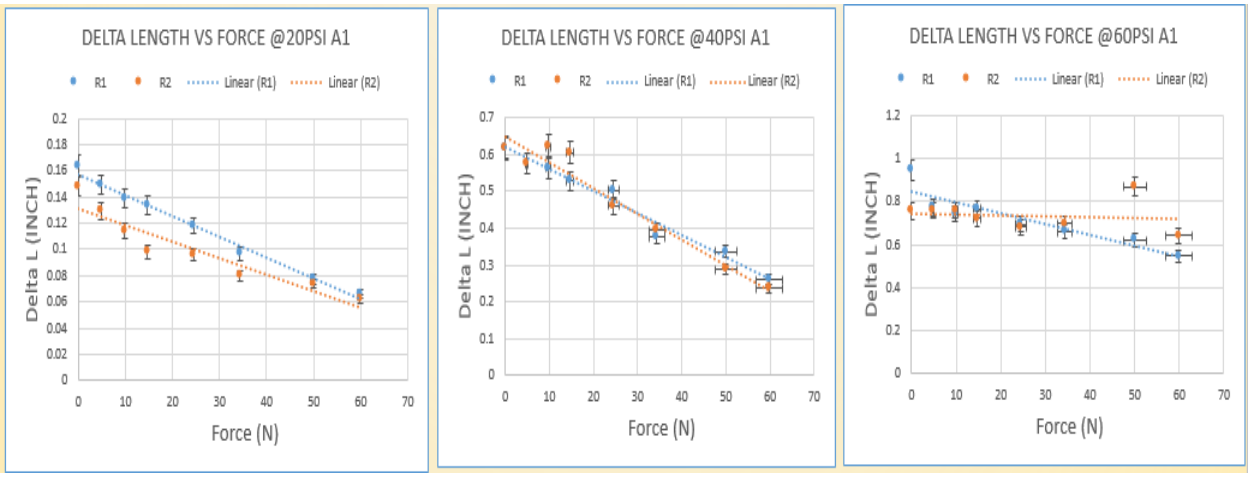

Figure 29: Comparison of maximum change in lengths (Delta L) at 20, 40, and 60 psi for air muscle A1.

All the three graphs plotted in the figure 30. below represents air muscle A2.

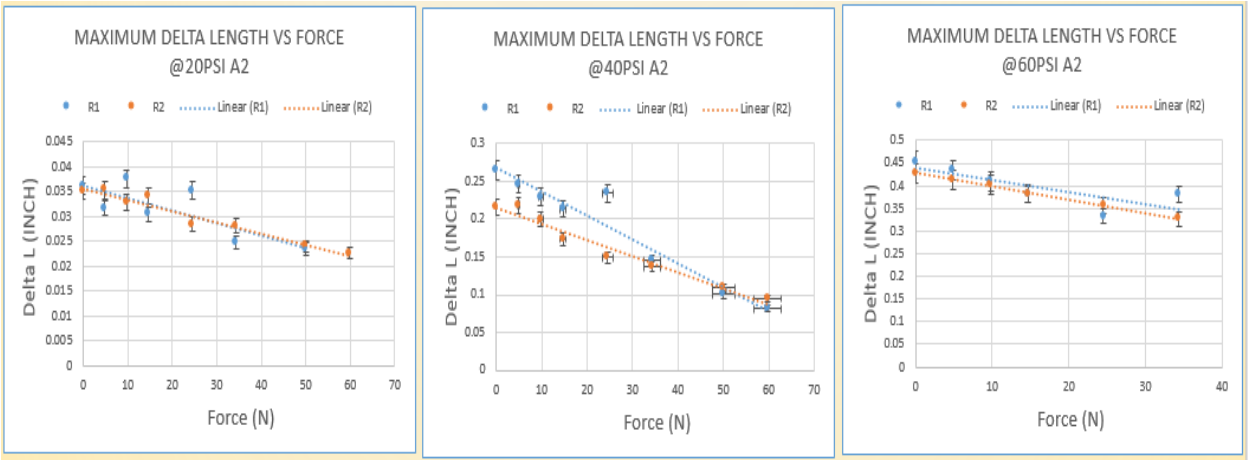

Figure 30: Comparison of Delta L at 20, 40, and 60 psi for air muscle A2.

.

Similar to the A1 graphs, in the first graph above, Delta L is plotted against the force at gauge pressure equal to 20 psi. The second and third graphs are plotted for the pressures equal to 40 psi and 60 psi, respectively.

In all the cases, as the force applied on the air muscles is increased, length of contraction (i.e., Delta L) decreases. For example, the maximum contraction for A2 at no load, R2, and 20 psi condition is about 0.035 in, while the same air muscle contracts only about 0.025 in when the force applied is 50 N.

Secondly, as the pressure is increased as seen in the second and third graphs the length of contraction for corresponding force is also increased. As with the no load condition, Delta L is at its max at 60 psi, around 0.45 in while at 40 psi it decreases to 0.27 in, and it drops further to just 0.035 in at 20 psi.

Once again it can be observed that reduction in volume flow rate does not affect the amount of contraction the air muscle undergoes.

The graphs in the figure 31. represent the maximum contraction length of air muscle A3 based on the different force applied on it. The first graph is plotted at 20 psi gauge pressure, while the measurements in the second graph are taken at 40 psi gauge pressure. As discussed earlier, the readings for A3 at 60 psi were not taken because Delta L was greater than the range of the linear potentiometer. The readings for air muscle A3 indicate the same observations that were made for air muscles A1 and A2: as the force applied on the air muscle is increased, Delta L decreases. It can also be observed that as the pressure is increased, Delta L increases.

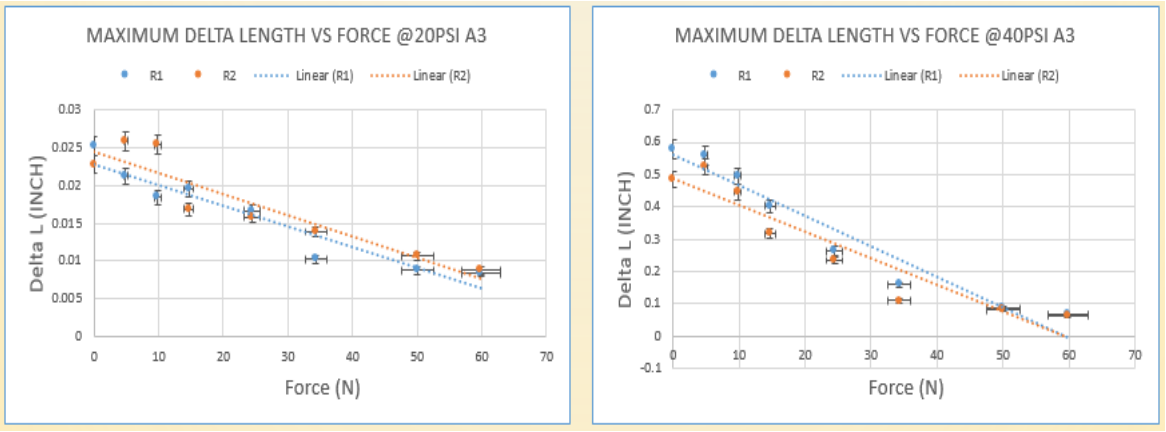

Figure 31: Comparison of Delta L at 20 and 40 psi for air muscle A3.

.

4. Theoretical Model to Quantify Relationship Between Velocity of Contraction and Force Applied on it.

4.1. Procedure:

Novel Approach to find the relationship between force and velocity in the proposed theoretical Model.

The first step of my research was the detailed study of theoretical modeling of air muscles. As per the equation for the pulling force applied by the air muscle by Chou, I derived the theoretical relation between force and the velocity of the contraction of the air muscle.

The force equation is given by

$$F = \frac{\pi {D_0}^2 P'}{4}(3cos^2\theta - 1) \qquad (34)$$

Following flowcharts on the next page describe the Static and Dynamic Models which are used to measure the velocity of contraction of the air muscles.

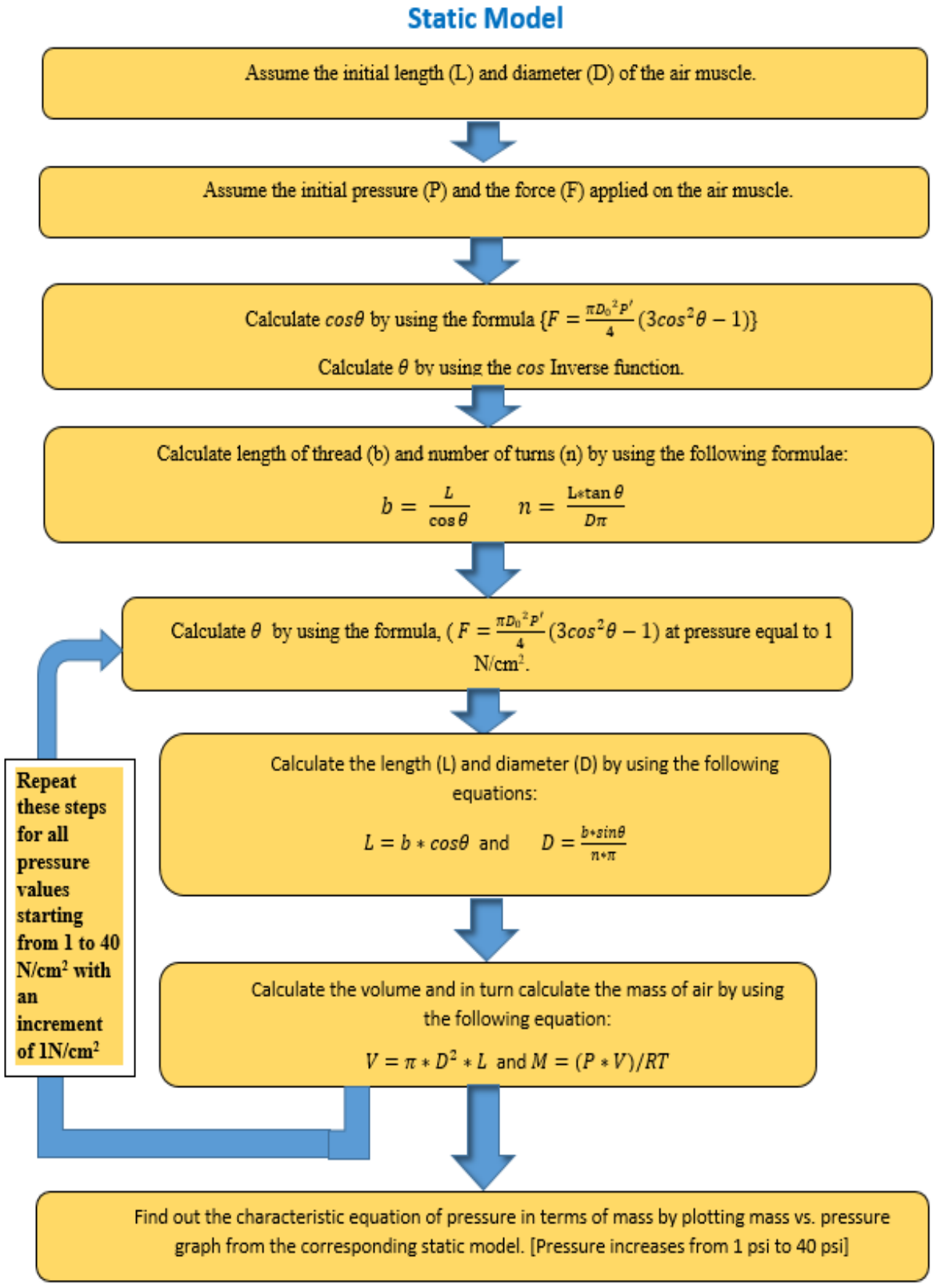

Figure 32: Static Model

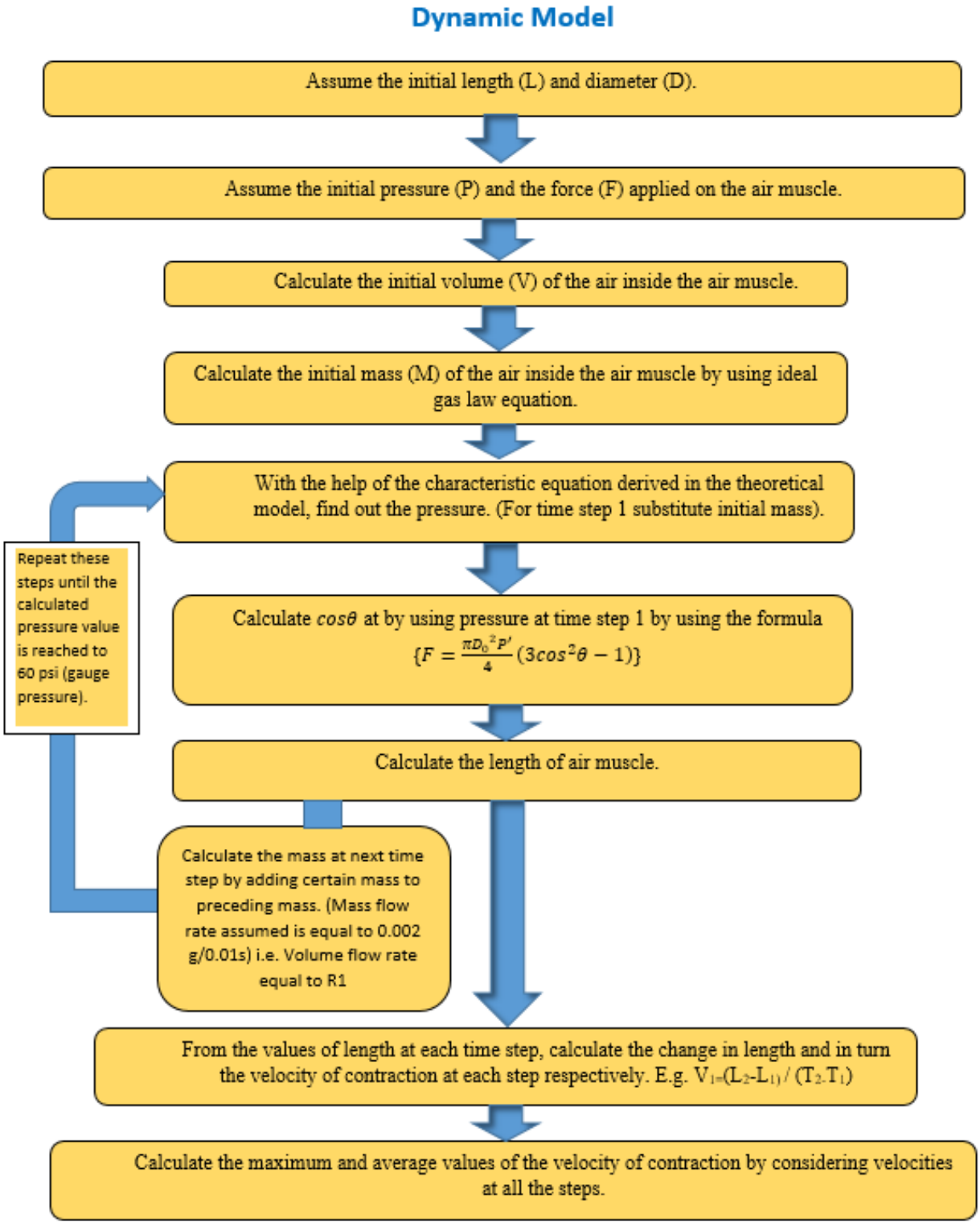

Figure 33: Dynamic Model

.

This theoretical model was implemented on the following six different load conditions:

Force applied = 10 N, 15 N, 25 N, 35 N, 50 N, and 60 N

The critical parameters of the air muscle on which the theoretical model was implemented were assumed as follows:

L1 (cm)	10
D1 (cm)	2
B (cm)	13.98
n	1.5
R	28.7
T	295
Initial V (cm^3)	31.4
Initial mass (grams)	0.05

The length and diameter of the air muscle in the model were assumed to be similar to one of the air muscles tested experimentally.

4.2. Results:

Here it is primarily indicated that how theoretical derived and experimental found results regarding length of the air muscle are similar. In the following graph displayed in figure 34, orange curve represents the theoretically measured length of the air muscle at force equal to 10 N and volume flow rate equal to R1 while blue curve represents the actual experimental length of the air muscle measured at the same load and volume flow rate set to restriction R1. In the graph displayed in figure 34. the blue line represents the theoretically measured length as a function of pressure. The orange line, on the other hand, represents the experimental data for the length against the gauge pressure. The force applied is 10 N in both the cases. Both the experimental as well as the theoretical curve show that as the pressure

.

increases to 40 psi, there is about 0.6 in of contraction. One more important point is that in both the cases, the air muscle starts to contract only after the pressure has gone above the threshold value, which is around 9 psi gauge pressure.

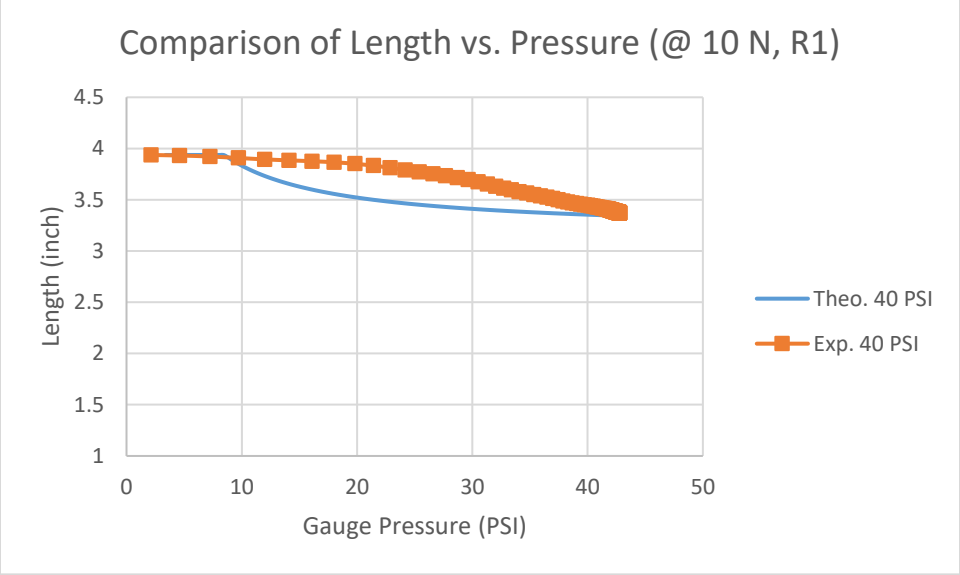

Figure 34: Comparison of theoretical versus experimental curves representing change in length plotted against the gauge pressure to actuate the air muscle.

With the help of the theoretical model, the graph in figure 35. plots the length of the air muscle against the pressure which is used to actuate the muscle. The model was operated for the following forces: 10 N, 15 N, 25 N, 35 N, 50 N, and 60 N, respectively. The model was not implemented at no force condition because, as per the force equation, zero contraction is yielded if input force is assumed as zero. However, in actual experiment if the even if zero force is applied on the air muscle certain contraction is observed. The initial length of the air muscle is assumed to be 3.92 in. As the pressure inside the air muscle is increased up to 60 psi, the air muscle gradually contracts. For example, in the case of a 1 N force, the initial length of the air muscle is 3.92 in at initial pressure. The length shortens to 3.3 in as the pressure is increased to 60 Psi. Hence, the total contraction observed is around 0.62 in. This clearly indicates that as the pressure is increased, the contraction of the air muscle also increases. Conversely, as the load is increased, the contraction decreases; hence, it can be

.

inferred that as the force applied on the air muscles is increased, the corresponding contraction is reduced.

This graph also illustrates the threshold pressure required to start the contraction movement for a specific load condition. This can be described as the pressure difference required to start the radial deformation of the rubber tube. The threshold pressure is result of the non-elastic deformation and the friction between the nylon sleeve and the rubber tube. [2]. Hence, we can see that, for a force of 10 N, the air muscle starts to contract when the pressure reaches 9 psi. However, in the case of 15 N force, the same air muscle starts to contract only once the pressure has reached 13 psi.

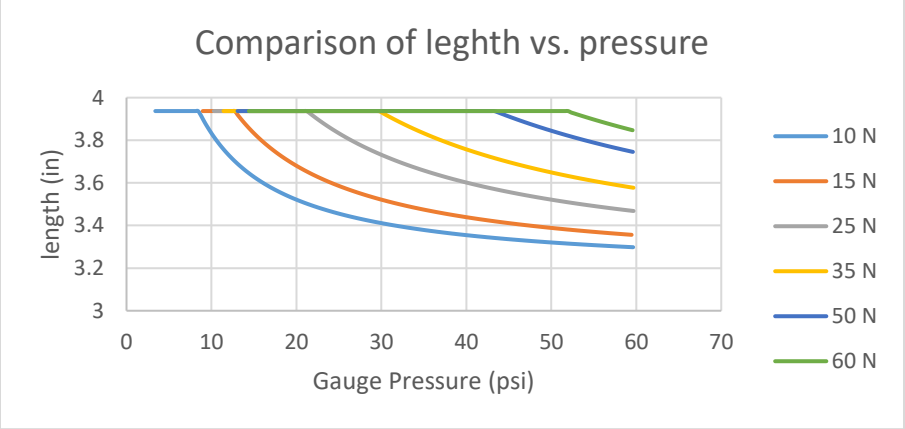

Figure 35: Comparison of change in length at different forces against the pressure activating the air muscle.

In the graph shown in figure 36. maximum length of contraction (i.e., Delta L) is plotted against the corresponding loads applied on the air muscle. The maximum contraction is measured with the help of the derived theoretical model.

As shown, as the force applied on the air muscle increases, the corresponding contraction of the air muscle decreases. When the force applied is 10 N, the air muscle is contracted by almost 0.62 in, while as the force increases to 60 N, the contraction is just about 0.1 in. Moreover, the trend line follows a linear path.

Additionally, figure 36. shows that even for the lower volume flow rate, the maximum contraction, i.e., Delta L, is constant. From this, it can be inferred that the reduction in velocity due to the reduction in volume flow rate is because it takes a longer time to achieve the

.

contracted length when mass flow is reduced, not because the contracted length is any different for the reduced mass flow case.

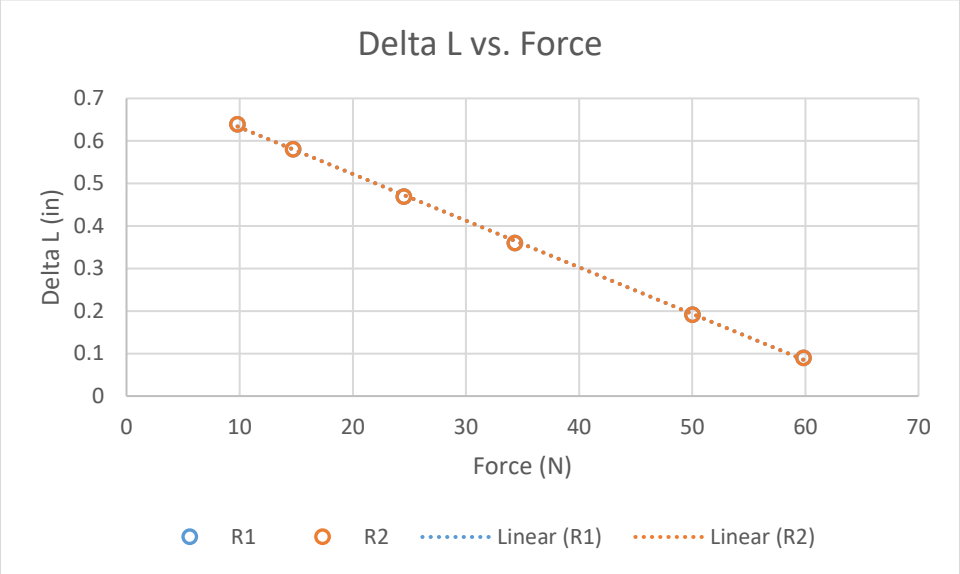

Figure 36: Comparison of Delta L vs. force at two different volume flow rates.

The following graph shown in figure 37. compares maximum velocities measured at different loads according to the theoretical model. It is the same theoretical model for calculating the Delta L in the earlier section.

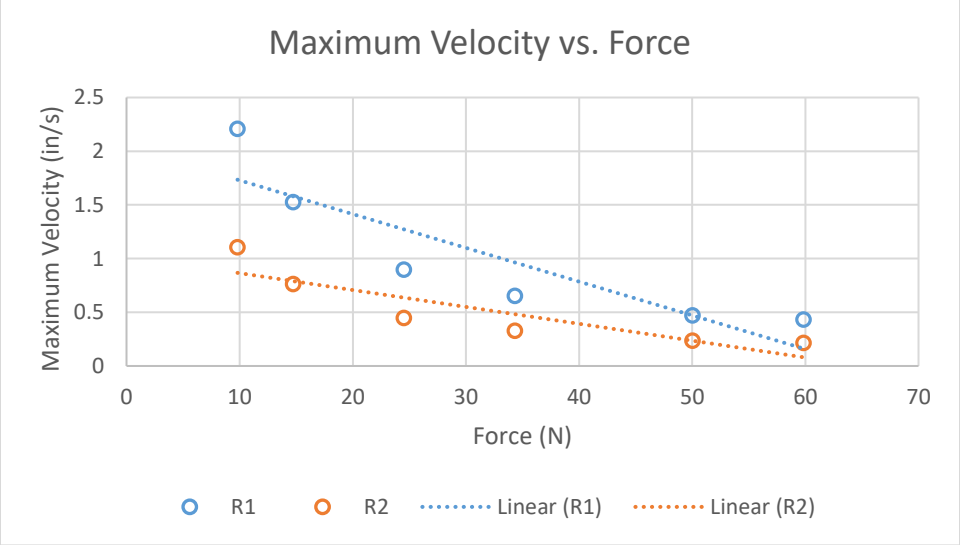

Figure 37: Comparison of maximum velocity vs. force at two different volume flow rates, denoted as R1 and R2.

.

Velocity of contraction is plotted for each time step with the help of the derived theoretical model. The pressure is increased up to 60 psi (gauge pressure). The velocities are plotted for two different volume flow rates. The volume flow rate is varied in the numerical model by adding a specific mass of air for each numerical time step. The theoretical model is operated for the loads ranging from 10 N to 60 N, i.e., from 10 N to 60 N, approximately. Maximum velocity of contraction is measured at each load at both volume flow rates. The second volume flow rate (R2) was induced by considering exactly half of the mass flow rate as compared to the to the first time (R1). The velocity of contraction is then measured in in/s, and the force is represented in Newtons (N).

Firstly, it can be clearly observed that as the force applied on the air muscles increases, the velocity of contraction decreases. In the case of volume flow rate 1 (R1), the maximum velocity at 10N is around 2.2 in/s while it reduced to 0.5 in/s at 60 N of force. The same result is even observed in the experiment where the velocity of contraction decreases when force increases. Secondly, it can be observed that when the same force is applied, the velocity of contraction is low for a smaller flow rate. This trend is consistent for all the forces ranging from 10 N to 60 N.

In these graphs shown in figure 38. the Delta L observed at different loads are plotted for 20 psi, 40 psi, and 60 psi gauge pressures. The three experimental curves are compared to the theoretical measured curve. Here, it can be seen that the air muscle contracts by 0.75 in at a force of 10 N when the experimental pressure is raised to 60 psi. However, only a 0.5 in of contraction is observed when 20 psi pressure is applied. Similar to the maximum velocity versus force plots, the theoretical curve and the experimental curve for 40 psi lie close to each other. All the trendlines show a linear nature. As seen in figure 38-b. even though the volume flow rate is reduced, the contraction of the air muscle remains constant. Both the experimental as well as the theoretical curves follow this trend.

.

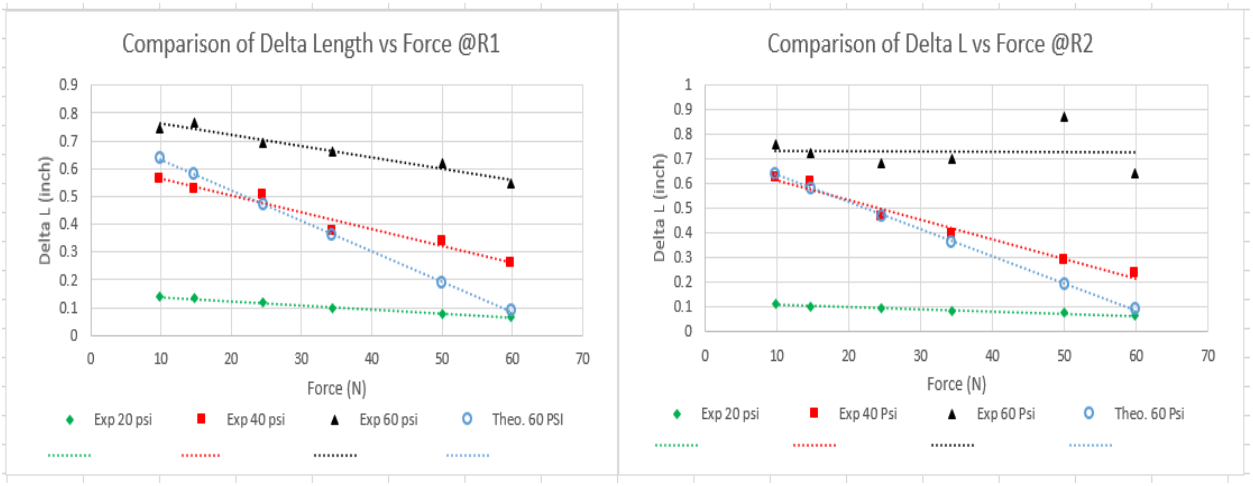

a. R1 b. R2

Figure 38: Comparison of Delta L vs. force at two different volume flow rates, denoted as R1 and R2.

Here in the figure 39. the maximum velocities measured by the theoretical model at different forces are compared with the maximum velocities measured experimentally at those forces, respectively. The same comparison is shown at a lower flow rate in figure39-b. Here, the theoretical modeled trendline is polynomial in nature, while the experimental trendlines are linear. All the curves show that as the force increases, the maximum velocity which can be achieved decreases. Yellow, red, and green lines represent measurements taken at gauge pressures of 60 psi, 40 psi and 20 psi, respectively. For example, in the case of the red line, the pressure entering the air muscle is increased from 0 to 40 psi for all the forces ranging from 0 to 60 N. In the case of the theoretical model, the pressure is increased from 0 to 60 psi for all of the forces. Thus, at greater pressures, greater maximum velocity is achieved. When the experimental pressure is 60 psi, the maximum velocity at 10 N force is around 4.3 in/s, while for the same force, only 0.5 in/s velocity is observed when the pressure is restricted to 20 psi. Consequently, and as might be expected, the maximum velocities achieved for 40 psi experimental pressure lie approximately between those of 60 and 20 psi. The theoretical measurements are closest to the 40 psi experimental readings: for a force of 10 N, maximum velocities for 40 psi are nearly about 2.2 in/s. The main reason for this is the assumed volume flow rate in the theoretical model. Therefore, it can be understood that by tweaking the volume flow rate, we can adjust the maximum velocity achieved for a specific force applied.

.

Additionally, by studying figure b, it can also be inferred that as the volume flow rate is lowered, the respective maximum velocities drop.

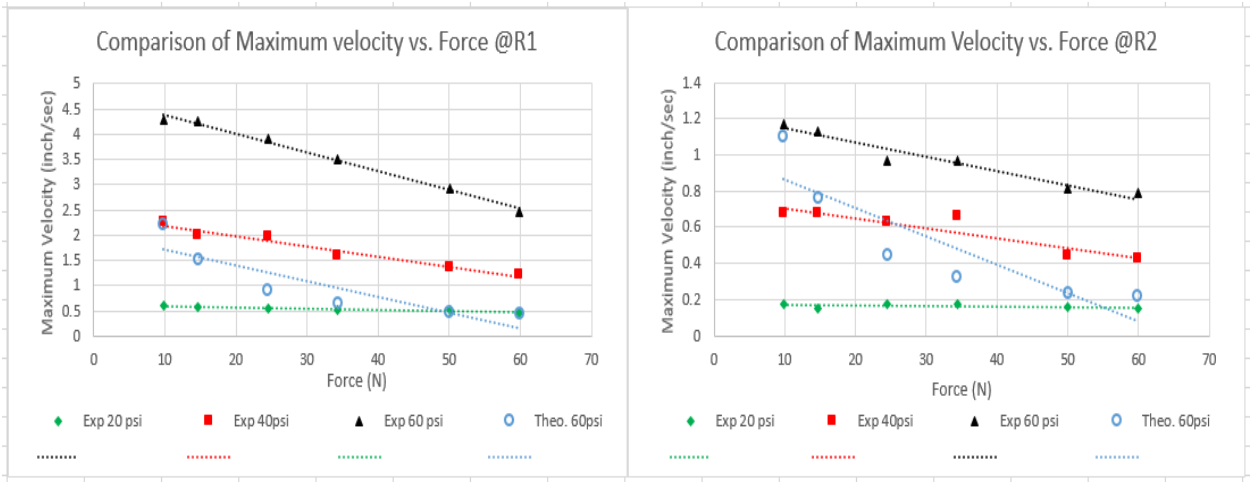

a. R1 b. R2

Figure 39: Comparison of maximum velocity vs. force at two different volume flow rates, denoted as R1 and R2.

.

5. Discussion:

This thesis paper primarily quantifies the relationship between velocity of contraction of air muscles and the force applied on it, which is a key characteristic of biological skeletal muscle. First, an experimental test rig was used to measure the velocity of contraction of air muscles as a function of applied force, supply pressure, and supply volumetric flow rate. Second, a theoretical model was proposed to quantify the relationship between the velocity of contraction and force applied on it and to explain the experimental results.

The first part of the experimental results compare the maximum and average velocities of three air muscles A1, A2 and A3 at 0N, 10N, 15N, 25N, 35N, 50N and 60N force conditions by taking into account two different volume flow rates. These graphs are plotted at 20 psi, 40 psi and 60 psi, respectively (see Figures 24, 26, and 28).

The contraction of the air muscle was measured with the help of a linear potentiometer. The range of the linear potentiometer used was 1 inch. As the contraction of air muscle A3 at 60 psi and at all the force conditions was more than 1 inch, the results for it are not considered.

At this point I would like to discuss the effect of initial length and initial diameter on the total length of the contraction (Delta L).

Length of air muscle is given by the following formula:

$$L = \left(\sqrt{\frac{\frac{4F}{\pi {D_0}^2 P'} + 1}{3}} \right) * b \qquad (39)$$

Therefore, we can say that L α (F, b/D_0^2, P').

However, Delta L = (L_0 −L).

Hence, Delta L α [L_0 - (F, b/D_0^2, P')].

From these equations, it is clear that Delta L (i.e., total length of contraction) is proportional to initial length and initial diameter.

.

It can be observed that at higher pressures (in this paper 60 psi) for air muscles having constant length, the smaller the diameter of the inner tube, the greater the contraction. However, as there are other factors like force, pressure, and length of the thread, the exact relation among amount of contraction, initial diameter and initial length is not developed in my study. The exact relationship would further help to accurately predict the velocity of contraction theoretically.

There are a few factors worth studying which would affect the relationship between the velocity of air muscles and forces applied on them. One important factor is the thickness of the air muscle (i.e., the overall thickness of rubber tube along with nylon mesh). Equation 36 actually gives us the formula for force applied on air if the thickness of the muscle is considered. Studying variations in thickness will help to predict exactly the amount of contraction that would be achieved if a certain force is applied on a certain type of air muscle. Friction between the braid strands is also one important factor which is not considered in my theoretical model. The nylon strands which are used to make the mesh move against each other and resisting force is caused due to the friction. The resisting frictional force causes loss of energy and hence the contractile force is reduced.

Also of interest are the properties of the rubber or silicone tube used to make the air muscle. Elasticity of the material, for instance, would have a major impact on the performance of the air muscle. Understanding these properties will further help to quantify accurate relationships between velocity of contraction and force applied on the air muscle.

The results in Figures 29, 30, and 31 show a linear relationship between velocity of contraction and force applied on air muscles. These trends can be helpful to predict the velocity of contraction at higher force by extrapolating the trendline. Similar to velocity, even Delta L vs. Force relationship is linear. Yet the graphs do show outliers. One of the reasons for these outliers is the noise due to the jerk applied on the linear potentiometer. The second reason might be the inbuilt variation in the linear potentiometer.

Figures 25, 27, and 29 demonstrate the relationship between maximum velocity of contraction and force applied on the air muscles. These bar charts help to demonstrate the relationship clearly since only 0N and 10N force conditions are taken into consideration. Also, the 0N comparison helps to understand the maximum velocity which can be achieved by an air muscle at certain pressure and volume flow rate conditions discussed in the paper.

.

Volume flow rate was controlled by a needle valve: the valve was either left fully open (R1) or it was only opened partially (R2). Even though the volume flow rate was not exactly measured, the needle valve enabled variance such that the effect of varying volume flow rate on the Delta L and the velocity of contraction could be discerned. From all the experiments, it can be clearly observed that as the volume flow rate is increased, velocity of contraction is increased, and vice versa. One reason this is important is because it affects the speed at which, say, the fingers of a prosthetic hand are actuated by air muscles. To achieve slow and gradual closing of the fingers, for instance, the volume flow rate of the air necessary to actuate the air muscles should be set low enough so that they contract slowly. On the other hand, for faster movements, the volume flow rate must be increased.

Another important finding is that at all the pressure and force conditions, Delta L remains constant, even if the volume flow rate is changed. Consider an example where a robotic arm has to be displaced by a fixed distance. Even though a fixed displacement of the robotic arm is required, any volume flow rate can be used to actuate the muscle so long as pressure is kept constant; the same displacement achieved each time, regardless of the volume flow rate.

The next important characteristic which can be observed is that as the pressure of the air to actuate air muscle is increased, the velocity of the air muscle is increased. Again, this characteristic is very important while designing a prosthetic hand or pick-and-place robotic arm. Consider an application where a prosthetic or pick-and-place robotic hand has to lift a delicate and lightweight object. The pressure of the air to actuate the air muscles, which in turn actuates the fingers of the robotic hand, should be set such that the contraction is slow and gradual enough not to give a jerk while picking up the object. Air muscle A1 contracts with a velocity of 0.8in/s at 20 psi while the velocity of contraction at 60 psi is about 4.2in/s at r1 and 0N force conditions. Refer figures 25 and 27.

It can be also observed that as the force applied on the air muscle is increased, Delta L and the velocity of contraction is decreased. Consider the air muscle A1. For a volume flow rate equal to R1 at a pressure of 20 psi, a Delta L equal to 0.16 in was recorded at 0N force while it was about 1 in at 10N force. At the same pressure and volume flow rate conditions, maximum velocity obtained at 0N force was 0.8 in/s while it was just 0.2 in/s at 10N force. Once again, consider an application where a robotic arm has to lift 10 kg load to a certain height. Here, while designing the arm, it is important to determine the correct volume flow

.

rate and pressure of the air actuating the air muscles, so that desired movement of the robotic arm would be achieved.

Theoretical model is also discussed in the paper which is proposed to quantify relationship between velocity of contraction and force applied by taking into effect of varying pressures and volume flow rates. These results were used to validate the experimental results.

The theoretical model was derived to calculate the velocity of contraction and to validate the experimental results. The model was operated for the following forces: 10 N, 15 N, 25 N, 35 N, 50 N, and 60 N, respectively. The model was not implemented at no force condition because, as per the force equation, zero contraction is yielded if the input force is assumed as zero. However, in the actual experiment even if zero force is applied on the air muscle, a certain contraction is observed.

In Figure 35, the length of the air muscle is plotted against the pressure which is used to actuate the muscle. The length is compared at different forces, as mentioned in the above paragraph. This graph illustrates the threshold pressure required to start the contraction movement for a specific load condition. This can be described as the pressure difference required to start the radial deformation of the rubber tube. According to Daerden and Lefeber the threshold pressure is the result of the non-elastic deformation and the friction between the nylon sleeve and the rubber tube [2]. Hence, we can see that, for a force of 10 N, the air muscle starts to contract when the pressure reaches 9 psi. However, in the case of 15 N force, the same air muscle starts to contract only once the pressure has reached 13 psi.

Even from the theoretical results, it is seen that as the volume flow rate is increased, velocity of contraction also increases. Also, as can be seen in Figures 36 and 37, Delta L remains constant even if the volume flow rate is changed, keeping pressure and force constant. Volume flow rate representing R1 is calculated by assuming mass flow rate equal to 0.002 g/s (mdot1) while R2 is calculated by assuming mass flow rate equal to exactly half of that of mdot1, i.e., equal to 0.001 g/s.

In Figure 38, theoretical and experimental results for maximum velocity of contraction are compared. The theoretical curve plotted for 60 psi pressure approximately overlaps the experimental curve for 40 psi. This can be explained by the fact that because experimental

.

R1 was not exactly measured, it might not be equal to the theoretically assumed volume flow rate R1. However, it is important to understand by studying these comparisons that one can achieve required velocity of contraction by appropriately setting volume flow rate to actuate the air muscle.

.

6. Conclusion:

The experimental rig allowed us to test different air muscles of varying sizes and shapes in order to calculate their maximum length of contraction and velocity of contraction at different pressure, force, and volume flow rate conditions. The derived theoretical model allowed us to predict the length of contraction as well as velocity of contraction at specific force, pressure and volume flow rate conditions if the initial size of the air muscle is known.

Summary of the results:

- The theoretical model as well as experimental results state that as the force applied on the air muscles increases, velocity of contraction and Delta L (maximum length of contraction) decreases.
- The velocity of contraction and Delta L both increase as a function of pressure.
- The velocity of contraction increases as a function of volume flow rate. This relation is due to the change in time, as the change in length remains constant at different volume flow rates.
- The change in length due to the contraction is related to pressure and volume flow rate and inversely proportional to the force applied.
- The change in length is proportional to both initial length and initial diameter.

The relationship between force and velocity is exciting and has potential for creating biomimetic actuators. The model from this experiment may be used to design actuators to have a force-velocity relationship. Air Muscles are light in weight and have a very good power-to-weight ratio. As PAMs are compliant in nature due to the compressibility of air, soft and safe interaction of the robotic arm can be achieved while handling fragile objects by controlling the operating pressure. However, PAM's have some drawbacks, too. Continuous supply air is required for smooth functioning of the robotic arm or dexterous hand. To maintain such air supply, an air reservoir is necessary, which makes mobility difficult. The fingers actuated by air muscles would have jerky movements, because starting and stopping the air supply create pulses in the system. Accurate positioning in the case of pick-and-place robots is hard to achieve because the expansion of the working fluid (i.e., air) can cause the

.

system to overshoot. In the case of a prosthetic hand, actuating air muscles can be dangerous, since a rupture in the air muscles can explode the mechanical components of hand. Hence, if improvement is done to overcome these drawbacks, especially for mobile robots having lightweight actuators, air muscles can be a better choice over electric drives.

.

7. References:

1. Daerden, Frank, and Dirk Lefeber. "The concept and design of pleated pneumatic artificial muscles." International Journal of Fluid Power 2.3 (2001): 41-50.

2. Daerden, Frank, and Dirk Lefeber. "Pneumatic artificial muscles: actuators for robotics and automation." European journal of mechanical and environmental engineering 47.1 (2002): 11-21.

3. Chou, Ching-Ping, and Blake Hannaford. "Measurement and modeling of McKibben pneumatic artificial muscles." Robotics and Automation, IEEE Transactions on 12.1 (1996): 90-102.

4. Ranjan, Ranjeet, P.K Upadhyay, Dr. Arbind Kumar, and Dr. Praveen Dhyani. "Theoretical and Experimental Modeling of Air Muscle."International Journal of Emerging Technology and Advanced Engineering 2.4 (2012). 1504-1508

5. 1,2R. Ramasamy, 2M.R. Juhari, 3M.R. Mamat, 2 S. Yaacob, 2N.F. Mohd Nasir and 4,5M. Sugisaka. “An Application of Finite Element Modeling to Pneumatic Artificial Muscle.” American Journal of Applied Sciences 2 (11): 1504-1508, 2005 ISSN 1546-9239 © 2005 Science Publications

6. Davis, Steve, and Darwin G. Caldwell. "Braid effects on contractile range and friction modeling in pneumatic muscle actuators." The International Journal of Robotics Research 25.4 (2006): 359-369.

.

7. Baldwin H. A. 1969. “Realization models of muscle function”. Proceedings of the Furdt rock Biomechanics Symposium, pp. 139- 148.

8. K. Inoue, "Rubbertuators and applications for robotics", Proceedings of the 4th International Symposium on Robotics Research, pp. 57–63, 1987.

9. B. Hannaford, J. M. Winters, C.-P. Chou and P. H. Marbot, "The anthroform biorobotic arm: a system for the study of spinal circuits", Annals of Biomedical Engineering, vol. 23, pp. 399–408, 1995.

10. J. J. Grodski and G. B. Immega, "Myoelectric control of compliance on a ROMAC protoarm", Proceedings of the International Symposium on Teleoperation and Control, pp. 297–308, 1988.

11. B. Tondu, V. Boitier and P. Lopez, "Théorie d'un Muscle Artificiel Pneumatique et application à la modelisation du muscle artificiel de McKibben", Comptes Rendus de l'Académie des Sciences, t.320 Série IIb, pp. 105–114. Académie des Sciences, France, 1995.

12. D. G. Caldwell, A. Razak and M. J. Goodwin, "Braided Pneumatic Muscle Actuators", Proceedings of the IFAC Conference on Intelligent Autonomous Vehicles, pp. 507–512, Southampton, 1993.

13. D. G. Caldwell, G. A. Medrano-Cerda and M. J. Goodwin, "Control of Pneumatic Muscle Actuators", IEEE Control Systems Magazine, vol. 15, number 1, pp. 40–48, 1995.

14. T. Hesselroth, K. Sarkar, P. P. van der Smaght and K. Schulten, "Neural network control of a pneumatic robot arm", IEEE Transactions on Systems, Man and Cybernetics, vol. 24, number 1, pp. 28–38, 1994.

.

8. Appendix:

8.1. Instruction Set to operate Experimental Test Rig.

1. Open the Instacal program on the computer and check whether the MC relay board is working properly.
2. Open the LabVIEW program and enter 10 in the millisecond multiple block in the front panel so that the time step for each successive reading is 0.01.
3. Check whether all the sensors are connected to the DAQ board properly. Also, ensure the connections of power supply, solenoid valve, and relay board.
4. Turn on the 12V and 10V power supplies to power the solenoid valve and the linear potentiometer.
5. Plug in the adapter of the signal conditioning boxes of the load cell and pressure transducers, respectively.
6. Turn on the shop air and, with the help of the pressure regulator, adjust the pressure of air entering the solenoid valve. Adjust the needle vale such that the volume flow rate is maintained at R1 or R2.
7. Attach the tray to the bottom of the air muscle to make the provision to adjust the load.
8. Once all these steps above are followed, the LabVIEW program is ready to run.
9. Staring with 20 psi and volume flow rate equal to R1, take eight measurements such that the force is increased from 0 N to 60 N.
10. Start the run button on front panel as the pressure, load, and volume flow rate conditions are properly set.
11. As soon as the program starts running, the readings from three sensors are acquired in the computer and the real-time readings can be seen in the respective windows. There is a provision on the front panel to select the file in which you can the save the readings.
12. Once the program starts running, press button 7, which turns on the solenoid valve. Once the solenoid valve is turned on, the air muscle is actuated as the pressurized air enters the air muscle. As the air muscle is actuated, it contracts and lifts the load. After

.

getting readings for two cycles of contraction and expansion each, press the stop button.

13. Automatically, the pressure vs. time and change in length vs. time graphs are plotted in the LabVIEW. Save the readings for each set of conditions in the selected Excel file.
14. Analyze the readings in the saved file to measure maximum and average of velocity of contraction and maximum contraction.
15. Follow steps 10–14 for all the settings of pressure and load.
16. Turn off all the devices, shut off the power supply, and close the program.

8.2. Raw Data Plots of Experimental Model:

These plots are plotted from the readings mentioned below. The readings are obtained for set up having specifications 40 psi with no load condition and restriction R1.

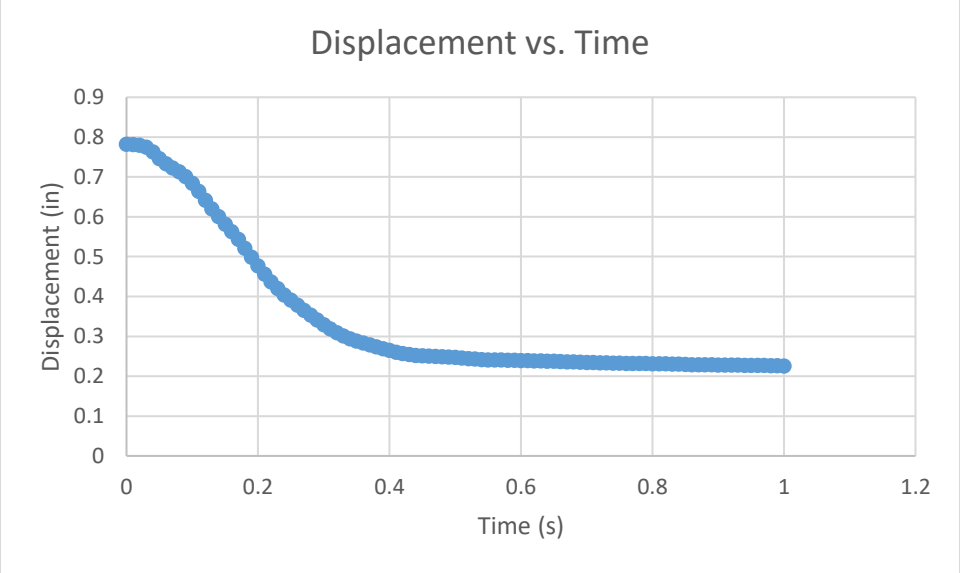

Figure: Time vs Displacement Plot of Experimental Data

.

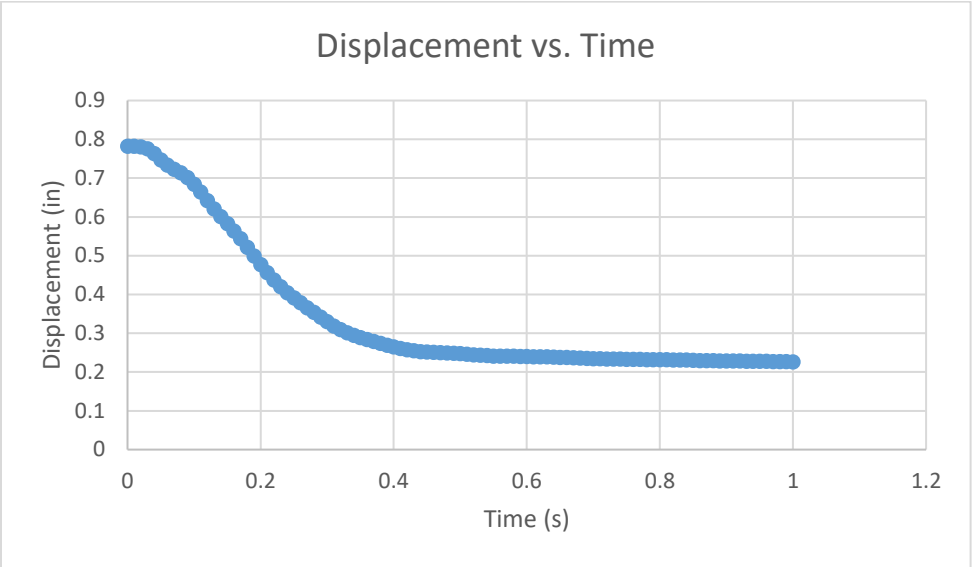

Figure: Time vs Velocity Plot of Experimental Data

From the above graphs maximum and average velocities for each case are measured.

8.3. Experimental Raw Data:

The following is the excel datasheet to plot the above graphs.

Raw Data Table for 40psi, 10N Force & R1 Condition Test for A1.			
Time (sec)	**Pressure (Psi)**	**Displacement (inch)**	**Velocity(inch/sec)**
0	2.18623	0.78208	0.0342
0.01	2.72119	0.781738	0.1806
0.02	5.57028	0.779932	0.4737
0.03	8.17293	0.775195	1.2109
0.04	10.55919	0.763086	1.6699
0.05	12.74109	0.746387	1.3379
0.06	14.79076	0.733008	1.0547
0.07	16.74425	0.722461	0.8936
0.08	18.60157	0.713525	1.2744

.

0.09	20.30261	0.700781	1.6845
0.1	21.83535	0.683936	2.0118
0.11	23.21181	0.663818	2.207
0.12	24.45002	0.641748	2.1435
0.13	25.62813	0.620313	1.9629
0.14	26.75213	0.600684	1.8799
0.15	27.81604	0.581885	1.875
0.16	28.81382	0.563135	1.9434
0.17	29.72745	0.543701	2.251
0.18	30.55693	0.521191	2.2461
0.19	31.32631	0.49873	2.1679
0.2	32.03558	0.477051	2.0655
0.21	32.72681	0.456396	1.9238
0.22	33.38799	0.437158	1.7187
0.23	34.0612	0.419971	1.5625
0.24	34.70435	0.404346	1.3282
0.25	35.33547	0.391064	1.289
0.26	35.93655	0.378174	1.2891
0.27	36.46549	0.365283	1.1816
0.28	36.97641	0.353467	1.211
0.29	37.4212	0.341357	1.1816
0.3	37.85397	0.329541	1.0986
0.31	38.26872	0.318555	0.9082
0.32	38.63537	0.309473	0.8399
0.33	39.01405	0.301074	0.6738
0.34	39.35666	0.294336	0.6104
0.35	39.66321	0.288232	0.4492
0.36	39.95773	0.28374	0.498
0.37	40.21019	0.27876	0.5078
0.38	40.43258	0.273682	0.4688
0.39	40.61892	0.268994	0.4199
0.4	40.76918	0.264795	0.4639
0.41	40.91344	0.260156	0.3027
0.42	41.00961	0.257129	0.249
0.43	41.13584	0.254639	0.2051
0.44	41.23802	0.252588	0.1123
0.45	41.32818	0.251465	0.0635
0.46	41.40031	0.25083	0.0635
0.47	41.4484	0.250195	0.1269
0.48	41.49648	0.248926	0.0781
0.49	41.53856	0.248145	0.0977
0.5	41.55659	0.247168	0.1465
0.51	41.58665	0.245703	0.1562
0.52	41.60468	0.244141	0.083
0.53	41.62271	0.243311	0.1172

.

0.54	41.66479	0.242139	0.1221
0.55	41.67681	0.240918	-0.0195
0.56	41.68883	0.241113	0.039
0.57	41.70085	0.240723	0.0342
0.58	41.7309	0.240381	0.0195
0.59	41.73691	0.240186	0.0489
0.6	41.74292	0.239697	0.0586
0.61	41.76697	0.239111	0.039
0.62	41.79702	0.238721	0.0049
0.63	41.80303	0.238672	0.0586
0.64	41.79702	0.238086	0.0488
0.65	41.82106	0.237598	0.044
0.66	41.84511	0.237158	0.0635
0.67	41.84511	0.236523	0.0537
0.68	41.85713	0.235986	0.0781
0.69	41.86915	0.235205	0.083
0.7	41.89319	0.234375	0.0146
0.71	41.91123	0.234229	0.0538
0.72	41.91123	0.233691	0.0048
0.73	41.91724	0.233643	0.044
0.74	41.92325	0.233203	0.0488
0.75	41.92926	0.232715	0.0293
0.76	41.97133	0.232422	0.0342
0.77	41.96532	0.23208	0.0146
0.78	41.97734	0.231934	0
0.79	41.98335	0.231934	0.0489
0.8	41.98937	0.231445	0
0.81	42.03144	0.231445	0.0244
0.82	42.01942	0.231201	0.0244
0.83	42.03144	0.230957	0.0391
0.84	42.03745	0.230566	0.0878
0.85	42.03745	0.229688	0.0928
0.86	42.04947	0.22876	-0.0097
0.87	42.05548	0.228857	-0.0147
0.88	42.07953	0.229004	0.0293
0.89	42.09155	0.228711	0.0195
0.9	42.09756	0.228516	0
0.91	42.09756	0.228516	0.0391
0.92	42.10357	0.228125	0.0244
0.93	42.11559	0.227881	0.0293
0.94	42.14564	0.227588	0.0049
0.95	42.15767	0.227539	0.0146
0.96	42.15767	0.227393	0.0293
0.97	42.15767	0.2271	0.0293
0.98	42.16368	0.226807	0.0244

.

0.99	42.1757	0.226563	0.0489
1	42.1757	0.226074	0.0879
1.01	42.19974	0.225195	0.0586
1.02	42.20575	0.224609	-0.0049
1.03	42.21176	0.224658	0.0732
1.04	42.21777	0.223926	0.0342
1.05	42.22378	0.223584	-0.0049
1.06	42.21777	0.223633	0.0098
1.07	42.23581	0.223535	0.0293
1.08	42.26586	0.223242	0
1.09	42.27788	0.223242	0.0097
1.1	42.27187	0.223145	0
1.11	42.27788	0.223145	0
1.12	42.27788	0.223145	0.0342
1.13	42.28389	0.222803	0.0391
1.14	42.2899	0.222412	0.0244
1.15	42.29591	0.222168	0.0293
1.16	42.31395	0.221875	0.0439
1.17	42.31395	0.221436	0.0293
1.18	42.33799	0.221143	0.0391
1.19	42.33799	0.220752	0.0049
1.2	42.33799	0.220703	0
1.21	42.33799	0.220703	0.0098
1.22	42.344	0.220605	0.0097
1.23	42.35602	0.220508	0.0098
1.24	42.35602	0.22041	-0.0049
1.25	42.37405	0.220459	0.0049
1.26	42.3981	0.22041	-0.0049
1.27	42.39208	0.220459	0.0098
1.28	42.3981	0.220361	0.0146
1.29	42.3981	0.220215	0
1.3	42.3981	0.220215	0.0635

8.4. Theoretical Model Data Sheet

Data sheet demonstrating the implementation of theoretical model to an air muscle to which a force equal to 10N has been applied.

	Load(kg)	1									
	accel	9.81			R	28.7					
	L1(cm)	10			T	295					
	D1	2			Initial V	31.4					

.

	b	10.928			mass	0.045					
	n	0.7016			Pressure	12.07	2.066	17.5			
	cosTheta	0.9151									
	theta	0.415									
mass (gram)	time (sec)	Gauge P(N/cm2)	Abs P (N/cm2)	Abs P (psi)	Cos θ (Rad)	θ (Rad)	Length cm	Diameter cm	volume cm3	Length (inch)	Velocity (inch/sec)
0.044	0	2.0658	12.0658	17.5	0.91512	0.415	10	2		3.937008	0.16678
0.105	0.054	2.0816	12.0816	17.523	0.91302	0.42	9.977	2.0234	32.066	3.928002	3.67084
0.109	0.108	2.4898	12.4898	18.115	0.86695	0.522	9.474	2.4723	45.455	3.729776	2.7621
0.113	0.162	2.898	12.898	18.707	0.83228	0.588	9.095	2.7499	53.987	3.580623	2.15856
0.117	0.216	3.3061	13.3061	19.299	0.80519	0.635	8.799	2.9417	59.77	3.464061	1.73597
0.121	0.27	3.7143	13.7143	19.891	0.7834	0.671	8.561	3.0831	63.876	3.370318	1.42791
0.125	0.324	4.1224	14.1224	20.483	0.76547	0.699	8.365	3.1919	66.9	3.293211	1.19606
0.129	0.378	4.5306	14.5306	21.075	0.75046	0.722	8.201	3.2785	69.193	3.228624	1.017
0.133	0.432	4.9388	14.9388	21.667	0.7377	0.741	8.061	3.349	70.974	3.173705	0.87572
0.137	0.486	5.3469	15.3469	22.259	0.7267	0.757	7.941	3.4076	72.385	3.126417	0.7622
0.141	0.54	5.7551	15.7551	22.851	0.71714	0.771	7.837	3.4571	73.523	3.085258	0.66958
0.145	0.594	6.1633	16.1633	23.443	0.70873	0.783	7.745	3.4995	74.454	3.049101	0.59299
0.149	0.648	6.5714	16.5714	24.035	0.70129	0.794	7.663	3.5362	75.226	3.017079	0.52892
0.153	0.702	6.9796	16.9796	24.627	0.69465	0.803	7.591	3.5683	75.873	2.988517	0.47476
0.157	0.756	7.3878	17.3878	25.219	0.68869	0.811	7.526	3.5966	76.42	2.96288	0.42856
0.161	0.81	7.7959	17.7959	25.811	0.68331	0.819	7.467	3.6218	76.888	2.939738	0.38883
0.165	0.864	8.2041	18.2041	26.403	0.67843	0.825	7.414	3.6443	77.29	2.918741	0.3544
0.169	0.918	8.6122	18.6122	26.995	0.67398	0.831	7.365	3.6645	77.639	2.899604	0.32437
0.173	0.972	9.0204	19.0204	27.587	0.66991	0.837	7.321	3.6829	77.944	2.882088	0.29802
0.177	1.026	9.4286	19.4286	28.179	0.66617	0.842	7.28	3.6995	78.212	2.865995	0.27476
0.181	1.08	9.8367	19.8367	28.771	0.66272	0.846	7.242	3.7147	78.448	2.851158	0.25414
0.185	1.134	10.245	20.2449	29.363	0.65953	0.851	7.207	3.7287	78.657	2.837434	0.23576
0.189	1.188	10.653	20.6531	29.955	0.65657	0.855	7.175	3.7415	78.844	2.824703	0.21931
0.193	1.242	11.061	21.0612	30.547	0.65382	0.858	7.145	3.7534	79.011	2.81286	0.20454
0.197	1.296	11.469	21.4694	31.139	0.65125	0.862	7.117	3.7643	79.162	2.801815	0.19121
0.201	1.35	11.878	21.8776	31.731	0.64885	0.865	7.09	3.7745	79.297	2.79149	0.17914
0.205	1.404	12.286	22.2857	32.323	0.64661	0.868	7.066	3.784	79.42	2.781816	0.16819
0.209	1.458	12.694	22.6939	32.915	0.64449	0.87	7.043	3.7928	79.532	2.772734	0.15821
0.213	1.512	13.102	23.102	33.507	0.64251	0.873	7.021	3.8011	79.633	2.764191	0.1491
0.217	1.566	13.51	23.5102	34.099	0.64064	0.875	7.001	3.8089	79.726	2.75614	0.14075
0.221	1.62	13.918	23.9184	34.691	0.63887	0.878	6.981	3.8162	79.811	2.748539	0.13309
0.225	1.674	14.327	24.3265	35.283	0.6372	0.88	6.963	3.823	79.889	2.741352	0.12604
0.229	1.728	14.735	24.7347	35.875	0.63562	0.882	6.946	3.8295	79.961	2.734546	0.11953
0.233	1.782	15.143	25.1429	36.467	0.63412	0.884	6.929	3.8356	80.027	2.728091	0.11352
0.237	1.836	15.551	25.551	37.059	0.63269	0.886	6.914	3.8414	80.088	2.721961	0.10795
0.241	1.89	15.959	25.9592	37.651	0.63134	0.888	6.899	3.8469	80.145	2.716132	0.10278
0.245	1.944	16.367	26.3673	38.243	0.63005	0.889	6.885	3.8521	80.198	2.710582	0.09797
0.249	1.998	16.776	26.7755	38.835	0.62882	0.891	6.871	3.857	80.247	2.705291	0.0935

.

8.5. LabVIEW Program Screen Shots.

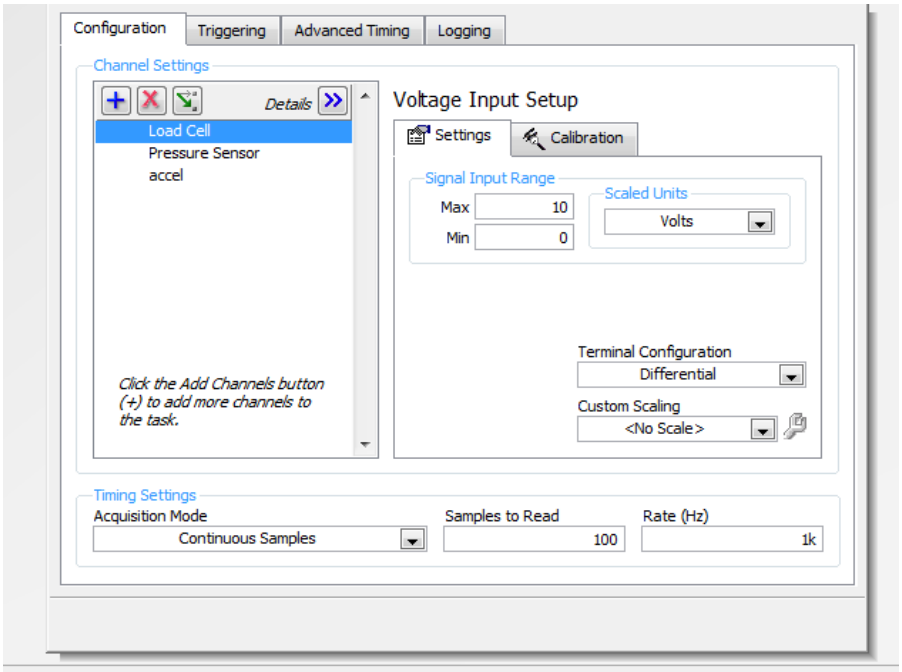

Figure: Configuration of Data Acquisition System.

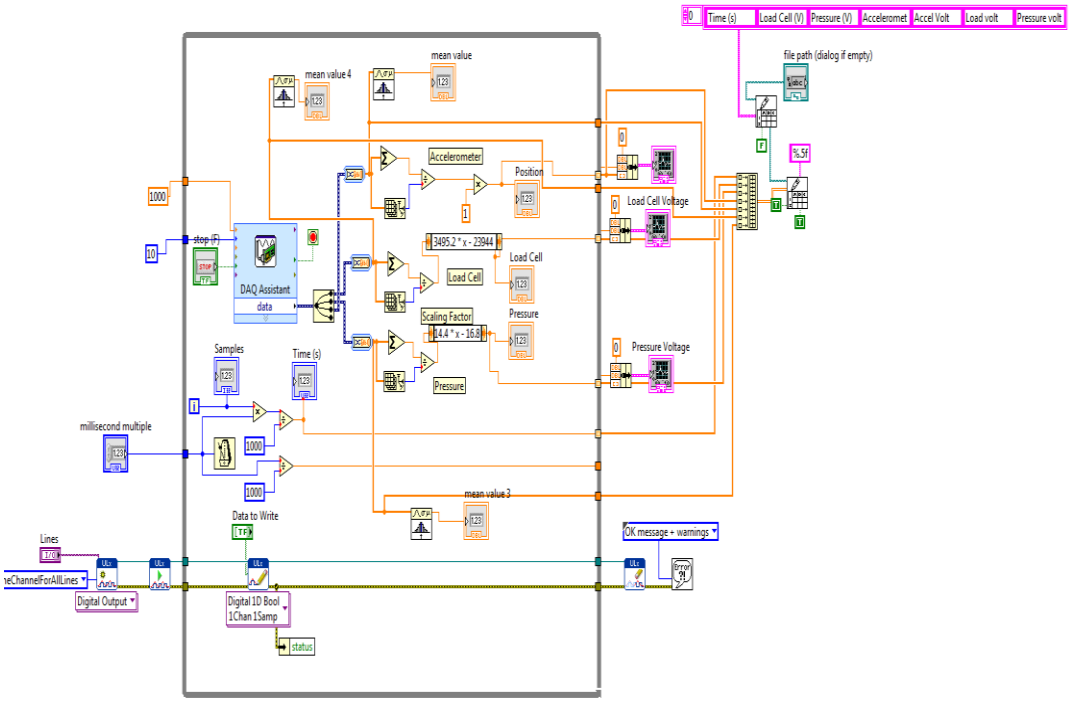

Figure: Back Panel, Block Diagram of the Program.

.

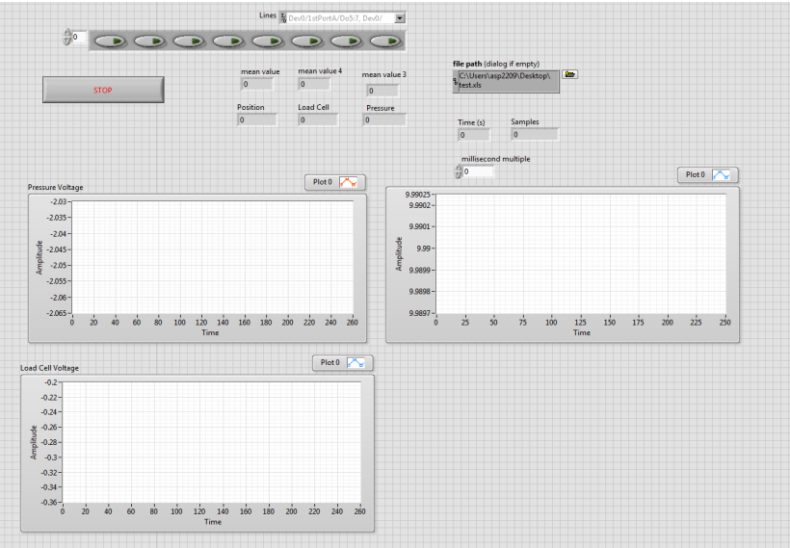

Figure: Front Panel of LabVIEW Program